

The kinetic Sunyaev-Zel’dovich signal from inhomogeneous reionization: a parameter space study

Andrei Mesinger^{1*}, Matthew McQuinn^{2†} & David N. Spergel³

¹*Scuola Normale Superiore, Piazza dei Cavalieri 7, 56126 Pisa, Italy*

²*Berkeley Astronomy Department, University of California, Berkeley, CA 94720, USA*

³*Department of Astrophysical Sciences, Princeton University, Princeton, NJ 08544, USA*

6 November 2018

ABSTRACT

Inhomogeneous reionization acts as a source of arcminute-scale anisotropies in the cosmic microwave background (CMB), the most important of which is the kinetic Sunyaev-Zel’dovich (kSZ) effect. Observational efforts with the Atacama Cosmology Telescope (ACT) and the South Pole Telescope (SPT) are poised to detect this signal for the first time, with projected $1 \mu\text{K}^2$ -level sensitivity to the dimensionless kSZ power spectrum around a multipole of $l = 3000$, $[\Delta_{l3000}]^2$. Indeed, recent SPT measurements place a bound of $[\Delta_{l3000}]^2 < 2.8 \mu\text{K}^2$ at 95% C.L., which degrades to $[\Delta_{l3000}]^2 < 6 \mu\text{K}^2$ if a significant correlation between the thermal Sunyaev-Zel’dovich (tSZ) effect and the cosmic infrared background (CIB) is allowed. To interpret these and upcoming observations, we compute the kSZ signal from a suite of ≈ 100 reionization models using the publicly available code 21CMFAST. Our physically motivated reionization models are parameterized by the ionizing efficiency of high-redshift galaxies, the minimum virial temperature of halos capable of hosting stars, and the ionizing photon mean free path – a parameterization motivated by previous theoretical studies of reionization. We predict the contribution of patchy reionization to the $l = 3000$ kSZ power to be $[\Delta_{l3000}^{\text{patchy}}]^2 = 1.5\text{--}3.5 \mu\text{K}^2$. Therefore, even when adopting the lowest estimate in the literature for the post-reionization signal of $[\Delta_{l3000}^{\text{OV}}]^2 \approx 2 \mu\text{K}^2$, none of our models are consistent with the aggressive 2σ SPT bound that does not include correlations. This implies that either: (i) the early stages of reionization occurred in a much more homogeneous manner than suggested by the stellar-driven scenarios we explore, such as would be the case if, e.g., very high energy X-rays or exotic particles contributed significantly; and/or (ii) that there is a significant correlation between the CIB and the tSZ. The later is perhaps not surprising, as massive halos should host both hot gas and star forming galaxies. On the other hand, the conservative SPT bound of $[\Delta_{l3000}]^2 \lesssim 6 \mu\text{K}^2$ is compatible with all of our models and is on the threshold of constraining physically motivated reionization models. The largest patchy kSZ signals correspond to an extended reionization process, in which the sources of ionizing photons are abundant and there are many recombinations (absorptions in sinks). We point out that insights into the astrophysics of the early Universe are encoded in both the amplitude and shape of the kSZ power spectrum.

Key words: cosmology: cosmic background radiation – dark ages, reionization, first stars – early Universe – diffuse radiation – large scale structure of Universe – early U

1 INTRODUCTION

Scattering of cosmic microwave background (CMB) photons off of inhomogeneities in the electron density after the recombination epoch imprints “secondary” anisotropies in the CMB. These secondaries are the dominant contribution to the CMB anisotropies at $\lesssim 5'$ scales. The largest and most studied of these secondaries is

the thermal Sunyaev-Zel’dovich (tSZ) effect, which results from Compton scattering off of $\sim 10^7$ K intracluster gas (Zeldovich & Sunyaev 1969), and most of the tSZ arises from $z < 1$ (e.g., Komatsu & Seljak 2002). The second most prominent is the kinetic Sunyaev-Zel’dovich (kSZ) effect and is the subject of this study. In contrast to the tSZ, the kSZ is not sourced by rare regions in the Universe but arises because most of the volume has a bulk peculiar motion with respect to the CMB frame (Sunyaev & Zeldovich 1980; Ostriker & Vishniac 1986; Vishniac 1987; Ma & Fry 2002). These motions impart a Doppler shift to the $\approx 10\%$ of CMB pho-

* email: andrei.mesinger@sns.it

† Einstein Fellow

tons that scatter after recombination. The kSZ is typically generated at higher redshifts than the tSZ, with a large fraction likely being sourced by inhomogeneities at $z \gtrsim 6$, during the epoch of reionization (Gruzinov & Hu 1998; Knox et al. 1998; Valageas et al. 2001; Santos et al. 2003; Salvaterra et al. 2005; McQuinn et al. 2005; Zahn et al. 2005).

Until recently, the prospects for detecting the kSZ were perceived by the CMB community as bleak. While the unique frequency dependence of the tSZ anisotropies should allow the separation of the kSZ from the tSZ, theoretical projections were that the tSZ signal would be more than an order of magnitude larger than that of kSZ on arcminute scales (e.g., Zahn et al. 2005). As such, instruments targeting the CMB secondaries would face the difficult task of using a limited number of frequency channels (~ 3) to isolate the much smaller kSZ signal while also using this frequency information to isolate the contamination from dusty galaxies and active galactic nuclei (Huffenberger & Seljak 2005). However, recent measurements have indicated that the amplitude of the tSZ power spectrum may actually be comparable to that of the kSZ rather than an order of magnitude larger. This lower value has been attributed to the lower σ_8 that is preferred by current cosmological measurements relative to the estimates of a few years ago (the amplitude of the tSZ power spectrum scales as $\sim \sigma_8^9$; Komatsu & Seljak 2002), and also to the realization that feedback processes strongly suppress the tSZ in clusters (Battaglia et al. 2010; Shaw et al. 2010; Trac et al. 2011). As a result, separating the two signals is now expected to be an easier task than had been anticipated.

Both the Atacama Cosmology Telescope (ATC)¹ and South Pole Telescope (SPT)² began measuring the CMB at arc-minute scales in 2007 and have recently published upper limits on the kSZ angular power spectrum (defined in Section 2). At present, the greatest challenge for these efforts is separating out several different terms that contribute to the angular power spectrum: the primordial CMB, the tSZ, radio sources, the cosmic infrared background (CIB), in addition to cross-power between the tSZ and radio sources, and between the tSZ and the CIB. The primordial fluctuations are important at low multiples and the sources (CIB/dusty galaxies and radio sources) are most important at high multipoles. The tSZ-CIB cross-correlation is currently the least understood component.

With ACT’s two frequency bands, Dunkley et al. (2011) placed a limit of $l^2/[2\pi][C_l^{\text{tSZ}} + C_l^{\text{kSZ}}] = 6.8 \pm 2.9 \mu\text{K}^2$ at the angular multipole of $l \approx 3000$, where C_l^{tSZ} and C_l^{kSZ} are the tSZ and kSZ angular power spectra, respectively. Using SPT’s three frequency bands and ignoring the tSZ-dusty galaxy correlation, Reichardt et al. (2011) recently reported an upper bound $l^2/[2\pi]C_l^{\text{kSZ}} < 2.8 \mu\text{K}^2$ at 95% C.L.. Reichardt et al. (2011) did note that the kSZ constraint is significantly weakened to $l^2/[2\pi]C_l^{\text{kSZ}} < 6 \mu\text{K}^2$ if this study allows for a significant anti-correlation between the tSZ and the cosmic infrared background. Analysis of the Planck data (Ade et al. 2011) suggest that 90% of the dust anisotropy power at $l \sim 3000$ is from $z > 2$ while simulations of the tSZ signal predict that the bulk of the signal is sourced from lower redshifts (Battaglia et al. 2011; Trac et al. 2011). While this Planck analysis argues that the tSZ-CIB cross-correlation is small, further work is needed to better characterize the redshift distribution of these signals as current models do not provide good fits to the Planck data (Shang et al. 2011). The detection of the kSZ

signal will likely require a combination of Herschel measurements of the dusty galaxies and multi-frequency millimeter observations by SPT and ACT. Nevertheless, even the recent conservative bound of $l^2/[2\pi]C_l^{\text{kSZ}} < 6 \mu\text{K}^2$ rules out the most extended reionization models in McQuinn et al. (2005).

The kSZ is comprised of two components: a component sourced primarily after reionization and referred to as the Ostriker-Vishniac (OV) effect (Ostriker & Vishniac 1986; Ma & Fry 2002)³ and a component from during reionization referred to as the patchy kSZ (Gruzinov & Hu 1998; Knox et al. 1998). The OV effect results from scattering off of density inhomogeneities with bulk peculiar velocities, with the fractional contribution per unit redshift peaking at $z \sim 1$ and monotonically decreasing with redshift above this peak. The OV is sourced by relatively linear scales, and it is likely that it can be modeled well enough to isolate the kSZ contribution from reionization. The patchy kSZ signal results from the order unity fluctuations in the ionized fraction that are anticipated by the vast majority of reionization models. Reionization also imprints other anisotropies in the CMB, primarily in polarization (Hu 2000; Doré et al. 2007; Dvorkin & Smith 2009; Su et al. 2011), which are not discussed here. However, other than the large-scale ($l \lesssim 10$) polarization anisotropies, the kSZ is by far the most detectable of the reionization-induced anisotropies.

The patchy kSZ anisotropies were originally calculated for several toy models of patchy reionization (Gruzinov & Hu 1998; Knox et al. 1998; Valageas et al. 2001; Santos et al. 2003). In the last several years, the kSZ from reionization has been calculated for more physically motivated models of reionization either using numerical simulations or semi-analytic models (Zahn et al. 2005; McQuinn et al. 2005; Iliev et al. 2007). Numerical simulations of reionization have not achieved large enough box sizes to both resolve this process and also capture the velocity flows which are correlated over hundreds of Mpc and which contribute significantly to the amplitude of the kSZ anisotropies (although, see Iliev et al. 2007 for a method to account for flows larger than the box size). More fundamentally, the heavy computational requirements of numerical simulations do not allow for exploration of the large astrophysical parameter space associated with reionization. Because of these limitations, recent years have seen the development of so called “semi-numerical” simulations of reionization, which incorporate an excursion-set model of reionization (Furlanetto et al. 2004) with large-scale realizations of the density field to produce 3D reionization morphology (Zahn et al. 2005; Mesinger & Furlanetto 2007; Geil & Wyithe 2008; Alvarez et al. 2009; Choudhury et al. 2009; Mesinger et al. 2011; Zahn et al. 2011). In this study, we use the publicly available 21CMFAST code⁴ to generate ~ 100 reionization scenarios in order to explore the parameter space of the patchy kSZ signal⁵.

There are many other potential probes of reionization, including: the CMB Thompson scattering optical depth, τ_e , (e.g., Komatsu et al. 2011); the redshifted 21cm line from neutral hydrogen (see, e.g., Furlanetto et al. 2006 and references therein); transmission statistics of quasar (QSO) spectra (e.g., Wyithe & Loeb

³ In some prior studies, “OV” has been used to refer to the linear-theory, post-reionization kSZ and the nonlinear theory was referred to as the “non-linear kSZ.” We do not adopt this terminology here.

⁴ <http://homepage.sns.it/mesinger/Sim.html>

⁵ When this work was nearing completion, a complementary study by Zahn et al. (2011) appeared in the literature. This study focused on constraining the duration and timing of reionization with recent SPT results. We will briefly compare our results to theirs in §4.

¹ <http://www.physics.princeton.edu/act/>

² <http://pole.uchicago.edu/>

2004; Mesinger & Haiman 2004, 2007; Fan et al. 2006; Bolton & Haehnelt 2007a; Maselli et al. 2007; Gallerani et al. 2008; McGreer et al. 2011; Bolton et al. 2011); intergalactic damping wing absorption in gamma-ray burst (GRB) spectra (Miralda-Escude 1998; Barkana & Loeb 2004; Totani et al. 2006; McQuinn et al. 2008; Mesinger & Furlanetto 2008a); the number density, clustering and evolution of Ly α emitters (LAEs; Malhotra & Rhoads 2004; Santos et al. 2004; Haiman & Cen 2005; Furlanetto et al. 2006; Malhotra & Rhoads 2006; Kashikawa et al. 2006; McQuinn et al. 2007; Dijkstra et al. 2007; Mesinger & Furlanetto 2008b; Iliiev et al. 2008; Dijkstra et al. 2011). However the CMB-based constraints are likely to be the only ones in the next decade that are capable of probing the highest-redshift part of reionization, $z \gtrsim 10$.

This paper is organized as follows. In §2, we summarize our method for estimating the kSZ signal. Our main results are presented in §3, namely the kSZ signal from a large range of reionization scenarios. In §4 we compare our results to previous works. In §5, we put our results in context with recent and forthcoming observations of the kSZ. Finally in §6 we present our conclusions.

Unless stated otherwise, we quote all quantities in comoving units. We adopt the background cosmological parameters $\{\Omega_\Lambda, \Omega_M, \Omega_b, n, \sigma_8, H_0\} = \{0.73, 0.27, 0.046, 0.96, 0.82, 70 \text{ km s}^{-1} \text{ Mpc}^{-1}\}$, consistent with the seven-year results of the *WMAP* satellite (Komatsu et al. 2011). We use the Fourier convention that is the standard in modern cosmological studies in which the 2π 's appear under the dk 's.

2 ESTIMATING THE KSZ SIGNAL

The CMB temperature anisotropy in the direction of the line-of-sight unit vector, $\hat{\mathbf{u}}$, can be written as:

$$\delta_T \equiv \frac{\Delta T}{T}(\hat{\mathbf{u}}) = \sigma_T \int dz c(dt/dz) e^{-\tau_e(z)} n_e \hat{\mathbf{u}} \cdot \mathbf{v}, \quad (1)$$

where σ_T is the Thomson scattering cross section, $\tau_e(z)$ is the Thomson optical depth to redshift z in the direction $\hat{\mathbf{u}}$, $\mathbf{v}(\hat{\mathbf{u}}, z)$ is the peculiar velocity, and $n_e(\hat{\mathbf{u}}, z)$ is the electron number density.

In our investigations, we split up the integral in eq. (1) into the post-reionization, low-redshift component – the OV signal – and the high-redshift, patchy kSZ reionization component. The patchy kSZ signal is defined in this study as the total kSZ from $z > 5.6$, even in cases for which reionization completed at redshifts higher than $z = 5.6$. However, the patchy reionization signal typically dominates the total kSZ from $z > 5.6$ and so this somewhat arbitrary definition makes little difference and facilitates the comparison of models. While the patchy kSZ signal is the focus of this paper, we discuss both the patchy and OV components in turn below.

We focus on characterizing the kSZ angular power spectrum $C_l^{\text{kSZ}} \equiv T_{\text{cmb}}^2 |\tilde{\delta}_T(k)|^2$, where $\tilde{\delta}_T$ is the Fourier transform of δ_T and $T_{\text{cmb}} = 2.73 \text{ K}$ is the temperature of the CMB. This statistic is the final analysis product of the relevant CMB observations. We will use the notation $[\Delta_l^{\text{kSZ}}]^2 \equiv l^2 C_l^{\text{kSZ}} / (2\pi)$. It is intuitive to relate in the flat sky approximation C_l^{kSZ} to the 3D ionization and density power spectra:

$$C_l^{\text{kSZ}} \approx \frac{T_{\text{cmb}}^2}{3} \int \frac{dn}{\eta^2} a^2 c^{-2} v_{\text{rms}}(z)^2 \sigma_T^2 \bar{n}_e(z)^2 \left[P_{xx}(z, \frac{l}{\eta}) + 2 P_{x\rho}(z, \frac{l}{\eta}) + P_{\rho\rho}(z, \frac{l}{\eta}) \right], \quad (2)$$

where we have also approximated the cosmological velocity flows

as coherent over much larger scales than those of interest, η/l where $l \approx 3000$ (e.g., Ma & Fry 2002). Here, η is the conformal distance from the observer, $v_{\text{rms}}(z)$ is the RMS amplitude of the peculiar velocity, and P_{XY} is the 3D cross power spectrum of the overdensity in X with the overdensity in Y , where the relevant overdensities are in the ionized fraction, x , and the density, ρ . During reionization the patchy term dominates, i.e., the term that arises from P_{xx} . In the absence of redshift evolution in the power spectra and the electron fraction, the integral in equation (2) grows as $(1 + z_{\text{max}})^{3/2}$ during matter domination, where z_{max} is the maximum integrated redshift. Thus, the same ionization topology at $z = 10$ contributes slightly more to the kSZ anisotropy than this topology at $z = 7$. More importantly, doubling the duration of the epoch when ionization structures are of a given scale approximately doubles the patchy kSZ signal, C_l^{patchy} , at that scale.

As a final remark, we have argued that reionization almost certainly occurred in a patchy manner, consisting of ionized and neutral regions. Even without any knowledge of P_{xx} other than that reionization was patchy – composed of zeros and ones –, there is an integral constraint on the reionization contribution to C_l^{kSZ} because the variance of the ionized fraction (or $x_i^{-1} - 1$, where x_i is the ionized fraction) must equal $\int k^2 dk / (2\pi^2) P_{xx}$. Thus, fixing the reionization history, $\int dl [\Delta_l^{\text{patchy}}]^2$ is a single number that is independent of the reionization morphology. This constraint suggests that smaller bubbles result in a smaller signal since $[\Delta_l^{\text{patchy}}]^2 \sim (\text{characteristic } l)^{-1} \sim \text{bubble size}$. However, the clustering of bubbles can invalidate this simple interpretation.

2.1 kSZ from patchy reionization

To model the patchy kSZ signal, we use the publicly available 21CMFAST code⁶. This code uses perturbation theory (PT) to generate the density and velocity fields, and PT plus the formalism of Furlanetto et al. (2004) to generate the ionization fields. We summarize these calculations below. For further details on these algorithms, see Mesinger & Furlanetto (2007) and Mesinger et al. (2011).

We first create a Gaussian random field in a simulation box which is 500 Mpc on a side, sampled onto a 1800^3 grid. This field is then mapped onto a lower-resolution 450^3 Eulerian grid at a given redshift using first-order Lagrangian PT (Zel' Dovich 1970) to compute what we refer to as the ‘‘nonlinear density field’’ and corresponding velocity field. The statistical properties of the density and velocity fields have been shown to match those from a hydrodynamic simulation remarkably well over the range of scales and redshifts relevant for patchy kSZ measurements (Mesinger et al. 2011).

Our ionization fields are generated directly from the nonlinear density field, with the excursion-set prescription of Furlanetto et al. (2004), slightly modified according to Zahn et al. (2011) (see their ‘‘FFRT’’ scheme). This algorithm marks regions as ionized for which the number of ionizing photons produced is greater than the number of neutral atoms. Specifically, a simulation cell at coordinate \mathbf{x} is flagged as ionized if

$$f_{\text{coll}}(\mathbf{x}, z, R) \geq \zeta^{-1}, \quad (3)$$

where ζ is an ionizing efficiency parameter (described later) and f_{coll} is the fraction of mass residing in dark matter halos inside a sphere of radius R and mass $M = 4/3\pi R^3 \rho$, where $\rho = \bar{\rho}[1 + \langle \delta_{\text{NL}} \rangle_R]$. This tabulation includes all halos above a set virial

⁶ <http://homepage.sns.it/mesinger/Sim.html>

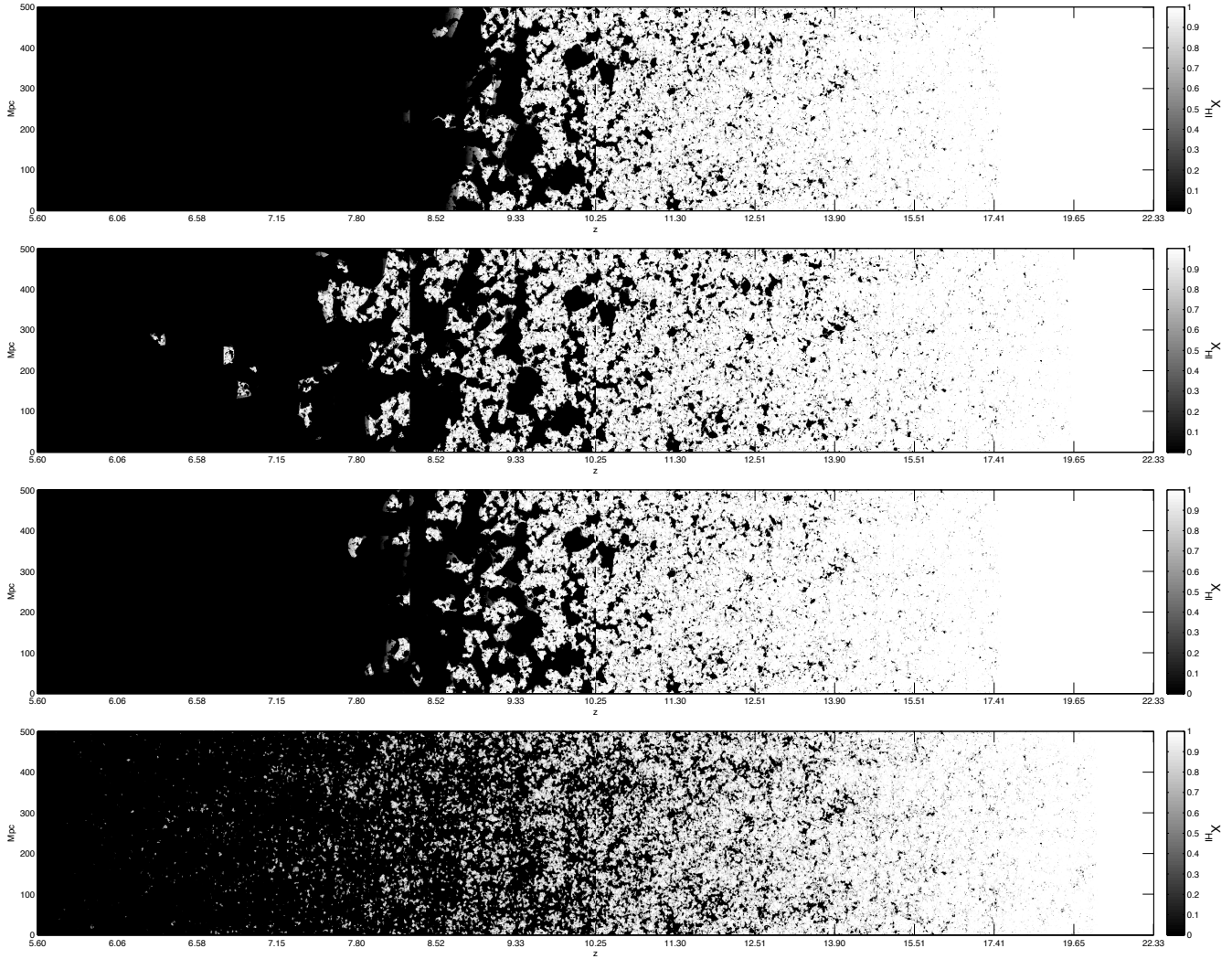


Figure 1. Slices through our ionization fields with thickness 1.1 Mpc. The top panel corresponds to $\{\zeta, T_{\text{vir}}, R_{\text{mfp}}\} = \{32, 10^4 \text{ K}, 60 \text{ Mpc}\}$. The middle two panels illustrate the impact of temporal evolution in our astrophysical parameters: $\{\zeta, T_{\text{vir}}, R_{\text{mfp}}\} = \{32[(1+z)/11]^2, 10^4 \text{ K}, 60 \text{ Mpc}\}$, and $\{\zeta, T_{\text{vir}}, R_{\text{mfp}}\} = \{32, 10^4 \text{ K}, 60 [7/(1+z)]^3 \text{ Mpc}\}$, from top to bottom. The bottom panel corresponds to an extreme scenario with a small mean free path, $\{\zeta, T_{\text{vir}}, R_{\text{mfp}}\} = \{32, 6.3 \times 10^3 \text{ K}, 3 \text{ Mpc}\}$. The models have $\tau_e = 0.087, 0.086, 0.085$, and 0.098 , consistent at 1σ with *WMAP*, and $[\Delta_{13000}^{\text{patchy}}]^2 = 2.4, 3.3, 2.5$, and $3.1 \mu\text{K}^2$ (top to bottom, respectively). The vertical lines that are sometimes evident (such as in the second panel at $z \approx 8.3$) owe to how the snapshots are stacked (see text for details).

temperature threshold, T_{vir} . We do not explicitly compute individual halo locations (as in Mesinger & Furlanetto 2007), but instead use the non-linear density field when computing f_{coll} (Zahn et al. 2011). Following the excursion-set approach (e.g., Bond et al. 1991; Lacey & Cole 1993), we iteratively decrease the scale R , starting from some maximum value, R_{max} , which we specify below as R_{mfp} . If at any R the criterion in equation (3) is met, this cell is flagged as ionized. We also take into account partially ionized cells by setting the cell’s ionized fraction to $\zeta f_{\text{coll}}(\mathbf{x}, z, R_{\text{cell}})$ at the last filter step for those cells which are not fully ionized. The resulting ionization fields are found to agree well with those generated with cosmological radiative transfer algorithms on scales relevant for the kSZ (Zahn et al. 2011; Mesinger et al. 2011).

We parameterize reionization with 3 free parameters:

(i) ζ : the ionizing efficiency of high-redshift galaxies. This quantity can be defined as $\zeta = f_{\text{esc}} f_* N_\gamma / (1 + n_{\text{rec}})$, where f_{esc} is the fraction of ionizing photons produced by stars that escape into

the intergalactic medium (IGM), f_* is the star formation efficiency, N_γ is the number of ionizing photons per stellar baryon, and n_{rec} is the mean number of recombinations per baryon. For reference, $f_{\text{esc}} = 0.1$, $f_* = 0.1$, $N_\gamma = 4000$ (appropriate for PopII stars), and $n_{\text{rec}} = 1$ yield $\zeta = 20$. However, the parameters f_{esc} and f_* are extremely uncertain in high-redshift galaxies (e.g., Gnedin et al. 2008; Wise & Cen 2009; Paardekooper et al. 2011). In this work, we explore the range $\zeta \sim 10\text{--}50$, which corresponds to what is consistent with CMB and Ly α forest constraints on reionization.⁷

⁷ Simple models at moderate redshifts find that a linear scaling between halo mass and UV luminosity, like the one used here (albeit for lower halo masses), provides a good fit to the observed galaxy luminosity function and their clustering properties (e.g., Vale & Ostriker 2006; Lee et al. 2009). Nevertheless, it is possible that the ionizing efficiency of galaxies varies significantly with halo mass at high redshifts. Since the dominant ionizing population at early times likely corresponds to a narrow range in halo

(ii) T_{vir} : the minimum virial temperature of halos that host the reionization sources. Much of the reionization literature sets this to $T_{\text{vir}} \approx 10^4$ K, the threshold temperature for efficient atomic cooling – corresponding to a halo mass of $M_{\text{halo}} \sim 10^8 M_{\odot}$ at $z \sim 10$. However, T_{vir} could be smaller than 10^4 K: The first stars were likely hosted by smaller halos with $M_{\text{halo}} = 10^{6-7} M_{\odot}$ (e.g., Haiman et al. 1996; Abel et al. 2002; Bromm et al. 2002). However, star formation inside such small halos was likely inefficient (with a handful of stars per halo), and was eventually suppressed by the heating from reionization itself or other feedback processes (Haiman et al. 2000; Ricotti et al. 2001; Mesinger et al. 2006; Haiman & Bryan 2006). T_{vir} could also have been larger than 10^4 K: Radiative and/or mechanical feedback (e.g., Springel & Hernquist 2003) eventually suppresses star formation inside $T_{\text{vir}} \lesssim 10^5$ K halos, though the details and timing of these processes are not well understood at high redshifts (e.g., Mesinger & Dijkstra 2008; Okamoto et al. 2008; Pawlik & Schaye 2009)⁸. Nevertheless, it is unlikely that T_{vir} is much greater than $\text{few} \times 10^5$ K, since these values approximately latch onto the faint end of the observed galaxy luminosity functions at $z \sim 6$ (e.g., Bouwens et al. 2008; Labbe et al. 2010; Salvaterra et al. 2011; Finlator et al. 2011). Additionally, high T_{vir} models have difficulty in latching onto the slow evolution of the observed emissivity, as inferred from the Ly α forest at $3 < z < 6$ (see Fig. 12 and associated discussion). Thus, we explore the range $T_{\text{vir}} = 10^3\text{--}3 \times 10^5$ K, which encompasses all conceivable T_{vir} .

(iii) R_{mfp} : the ionizing photon mean free path within ionized regions of the IGM. The mean free path to intersect an optically thick system (termed Lyman Limit Systems; LLSs) is measured to have been $R_{\text{mfp}} \sim 50$ comoving Mpc at $z = 6$, albeit with order-unity uncertainty (e.g., Storrie-Lombardi et al. 1994; Stengler-Larrea et al. 1995; Péroux et al. 2003; Prochaska et al. 2009; Songaila & Cowie 2010). This parameter becomes important in our models when the ionized region size R is larger than R_{mfp} , resulting in most of the ionizing photons being absorbed in LLSs rather than in the diffuse IGM, thereby retarding reionization. Thus, the smallest values for R_{mfp} have the largest impact in our models.⁹ In this work, we explore the range $R_{\text{mfp}} = 3\text{--}80$ Mpc.

Our parameterization ignores redshift evolution of the above astrophysical parameters. Since reionization is expected to have been extended, it is in fact likely that there would have been some evolution in these parameters. However, we find that only a fraction of the reionization history contributes the bulk of the patchy kSZ signal, making evolution less important. Nevertheless, we also investigate a few scenarios that have evolving parameters.

In order to explore the patchy kSZ signal in this 3 parameter volume, we have simulated 103 different reionization models. The ionization boxes for each model are computed at redshift intervals of $\Delta z = 0.2$, spanning the redshift range $z = 5.6\text{--}22.4$. This

masses (because of the steepness of the halo mass function), a halo mass-independent value of ζ may still be a good approximation.

⁸ Note that the combination of mechanical and radiative feedback, which by themselves likely have different mass-scalings, could conspire to create a relatively flat (i.e., with weak halo mass dependence) suppression of star formation (e.g., Finlator et al. 2011). Such an effect most appropriately translates to a lower value of ζ (e.g., by lowering f_*).

⁹ Note that in our simple model, the mean free path is spatially homogeneous. There are likely inhomogeneities in R_{mfp} during reionization, though the extent of these inhomogeneities is currently unknown (e.g., Choudhury et al. 2009; Crociani et al. 2011; McQuinn et al. 2011).

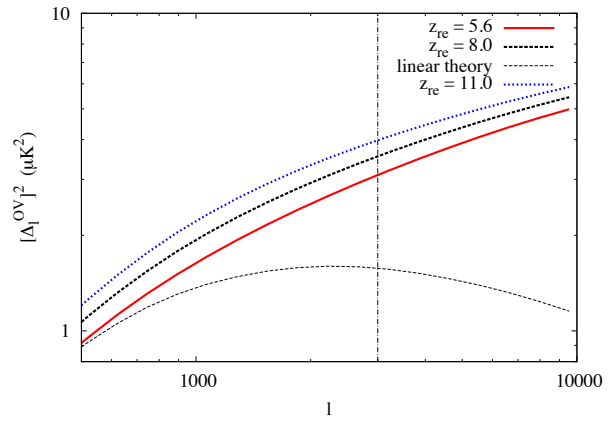


Figure 2. OV dimensionless angular power spectrum for instantaneous reionization scenarios with a reionization redshift of $z_{\text{re}} = 5.6$ (solid curve), 8 (dashed), and 11 (dotted). We have also plotted the OV power spectrum calculated in linear theory for the $z_{\text{re}} = 8$ case.

procedure generates 85 ionization boxes for each parameter combination, with the entire ≈ 100 -point parameter space being sampled in roughly one week on an 8-core desktop computer. We interpolate the density, velocity and ionization fields linearly in cosmic time between two consecutive simulation outputs. As is traditionally done in secondary CMB anisotropy calculations, we rotate the boxes when reaching their edges so as to minimize coherent stacking of the signal. Sample slices through four simulations are shown in Fig. 1. We have performed box size and resolution tests with a fiducial model and found convergence in the $l \sim 2000\text{--}10000$ kSZ power to $\approx 10\%$ (see Appendix A).

2.2 The post reionization kSZ

The kSZ from after reionization – which we refer to as the OV effect – is a contaminate for studying the patchy kSZ signal. Any modeling uncertainty in this post-reionization component will bias constraints on the patchy component. At $l \approx 3000$, the OV anisotropy contributed per unit redshift peaks at $z \approx 1$ and falls off weakly towards higher redshifts (becoming zero when there are no longer free electrons around). Figure 2 shows the OV anisotropies for three instantaneous reionization scenarios with reionization redshifts of $z_{\text{re}} = 5.6, 8,$ and 11 . We find the amplitude of the OV dimensionless (i.e. without units of length) angular power spectrum at $l = 3000$ to be $[\Delta_{l3000}^{\text{OV}}]^2 = 3\text{--}4 \mu\text{K}^2$.

These curves were calculated using the pseudo-nonlinear formula for the OV derived in Ma & Fry (2002) (a more accurate expression than in eq. 2). This calculation takes the linear theory OV calculation of Vishniac (1987) and substitutes a nonlinear theory for the density field, here computed from the Peacock and Dodds density power spectrum (Peacock & Dodds 1994).¹⁰ At higher multipoles than $l = 3000$, this suppression is more significant. For reference, $\eta 2\pi/l = \{4, 7, 14, 20\}$ Mpc at $z = \{0.5, 1, 3, 10\}$

¹⁰ In our calculation, we use linear perturbation theory for the velocity field, an approximation justified in Ma & Fry 2002. In addition, we note that the density power spectrum has not been “filtered” in our calculations to account for the pressure smoothing of the baryons (as was done in McQuinn et al. 2005 and references therein), but note that this should have little effect at the multipole of interest, $l = 3000$, unless there is significant feedback. We verified this for the window function measured in Shaw et al. 2011, e.g. their eq. (21), which we find suppresses the power at $l = 3000$ by only a few percent.

at $l = 3000$. The fact that these are pseudo-linear scales is why the linear theory calculation only differs from the nonlinear calculation by a factor of ≈ 2 (compare the dashed curves in Fig. 2, which correspond to the linear and nonlinear OV for $z_{\text{re}} = 8$). This relatively small difference suggests that the modeling uncertainty is less severe for the OV compared to, for example, the highly nonlinear thermal SZ.

How do our analytic predictions for the OV compare with those in numerical simulations? As mentioned in the introduction, simulating the kSZ is notoriously difficult (e.g., Zhang et al. 2004), and most numerical calculations of the OV should be considered lower limits on this signal owing to missing large-scale velocity modes. However, some recent simulations have achieved box sizes where they should be capturing the large-scale velocity flows. Of note, Trac et al. (2011) investigated the OV assuming a similar cosmology as is used here and found a signal that ranged between $[\Delta_{l=3000}^{\text{OV}}]^2 = 1.8 - 2.4 \mu\text{K}^2$ at $l = 3000$ for $z_{\text{re}} = 10$ in the four scenarios they investigated. (The lowest value in this range was from a simulation with a strong feedback prescription.) A similar range of values was found in Shaw et al. (2011), who argued that baryonic physics/feedback could suppress the kSZ by a maximum of $1 \mu\text{K}^2$ from our fiducial estimates that do not include such effects. We adopt this number as the maximal suppression in the OV from our calculations, i.e., $[\Delta_{l=3000}^{\text{OV}}]^2 > 2 \mu\text{K}^2$.

We henceforth only plot the kSZ power that originates from $z > 5.6$, which is dominated by the patchy component of the kSZ. We have argued that the $z < 5.6$ contribution has $[\Delta_{l=3000}^{\text{OV}}]^2 \equiv 3000^2 C_{l=3000}^{\text{OV}}/2/\pi \approx 2-3 \mu\text{K}^2$ at $l = 3000$. This range is one-third to half of the conservative $< 6 \mu\text{K}^2$ bound of SPT (Reichardt et al. 2011), resulting in the constraint $[\Delta_{l=3000}^{\text{patchy}}]^2 \equiv 3000^2 C_{l=3000}^{\text{patchy}}/2/\pi < 3 - 4 \mu\text{K}^2$. However, the more aggressive bound of $[\Delta_{l=3000}^{\text{patchy}}]^2 < 3 \mu\text{K}^2$ from Reichardt et al. 2011 would imply $[\Delta_{l=3000}^{\text{patchy}}]^2 < 1 \mu\text{K}^2$.

3 RESULTS

3.1 Power spectra and physical intuition

In this section we present the kSZ signal is several of our models. Qualitatively a few trends are anticipated. First, early and extended reionization scenarios should have a larger kSZ signal. Second, the peak in ionization power shifts from small to large scales as reionization progresses and the HII bubbles grow (e.g., McQuinn et al. 2007). Therefore the kSZ power at higher multipoles probes earlier epochs (see Fig. 4).

To quantify these trends, we begin by showing the patchy kSZ angular power spectra for a sample of reionization models. Fig. 3 shows how the kSZ power spectra change as we vary ζ (*top panel*), R_{mfp} (*middle panel*), and T_{vir} (*bottom panel*). The inset in each panel shows the associated reionization history. Unless specified otherwise, the parameter values for each curve are $\{\zeta, T_{\text{vir}}, R_{\text{mfp}}\} = \{42, 10^4 \text{ K}, 60 \text{ Mpc}\}$.

Increasing the ionizing efficiency parameter, ζ , quickens the progress of reionization as galaxies are more efficient ionizers of the IGM. The differences in the reionization histories (\bar{x}_{HI} at fixed z) increase with time (decreasing redshift). Therefore changing ζ has the most significant impact on the smallest multipoles (larger spatial scales) that are shown, since these multipoles are sourced by the later stages when ionized structures were large.

Changing the mean free path of ionizing photons, R_{mfp} , primarily impacts the middle and late stages of reionization. Small

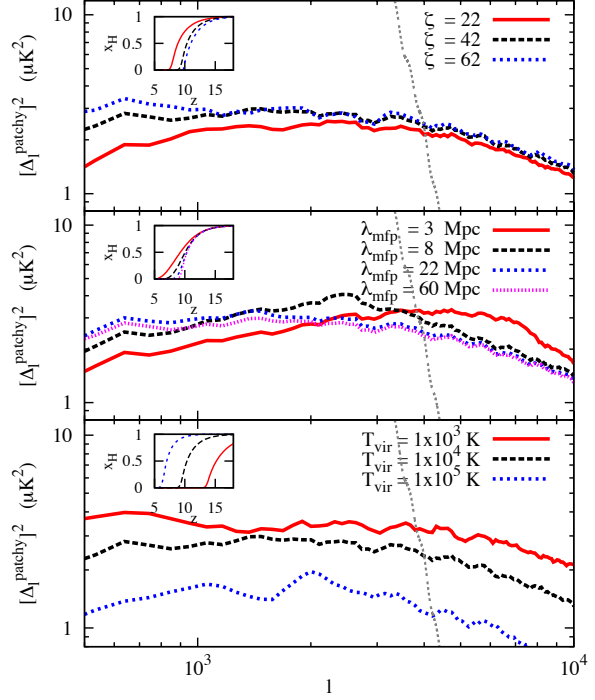


Figure 3. The dimensionless angular power spectrum of the patchy kSZ, $[\Delta_{l}^{\text{patchy}}]^2$, as ζ , R_{mfp} , and T_{vir} are separately varied around $\{\zeta, T_{\text{vir}}, R_{\text{mfp}}\} = \{42, 10^4 \text{ K}, 60 \text{ Mpc}\}$, (top, middle, and bottom panels, respectively). The inset in each panel shows the associated reionization history. The near-vertical gray dashed line corresponds to the primary CMB anisotropies (which are understood well enough that their contribution can be isolated at $l \gtrsim 2500$).

values of R_{mfp} extend the end of reionization as seen in the inset in the middle panel of Fig. 3 (c.f. Furlanetto & Mesinger 2009; Alvarez & Abel 2010). When the size of the ionized bubbles approaches R_{mfp} , reionization is slowed as ionizing photons become increasingly swallowed by photon sinks instead of pushing out the edges of the HII regions. Remaining neutral regions must then be ionized by local sources. We see that for this fiducial model where atomically cooled halos host ionizing sources, the mean free path only affects the kSZ signal when $R_{\text{mfp}} \lesssim 15 \text{ Mpc}$. As R_{mfp} is decreased (particularly to the smallest values considered), the peak of the patchy kSZ power spectra shifts to smaller scales.¹¹

Increasing T_{vir} delays reionization until the halos above this virial temperature threshold can form in sufficient abundance (bottom panel, Fig. 3). Increasing T_{vir} also results in a more sudden reionization as the number of halos with time grows more quickly as the halos become rarer.

In Fig. 4, we present the kSZ power spectra corresponding to the four models shown in Fig. 1. The total signal is represented by the solid red curves, with dashed curves showing the contributions up to the specified redshift. The top panels in both figures 1 and 4 correspond to a non-evolving model with $\{\zeta, T_{\text{vir}}, R_{\text{mfp}}\} = \{32, 10^4 \text{ K}, 60 \text{ Mpc}\}$. The second panels down correspond to the same parameters as the top panels, but including redshift evolution

¹¹ One might worry that $R_{\text{mfp}} = 3 \text{ Mpc}$ is only a factor of ≈ 3 larger than our cell size. To test whether this resolution limit has a quantitative impact on our results, we ran a higher resolution, 750^3 , run with the same astrophysical parameters as the model featured in the bottom panel of Fig. 1, and found good convergence (see Appendix A).

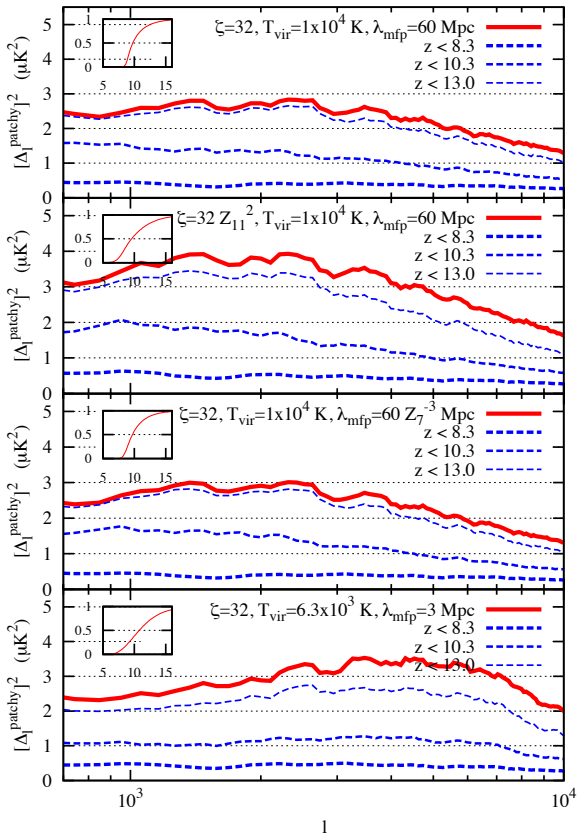


Figure 4. The kSZ dimensionless angular power spectra for the models featured in Fig. 1. The inset in each panel shows the evolution of \bar{x}_{HI} (y-axis) with redshift (x-axis).

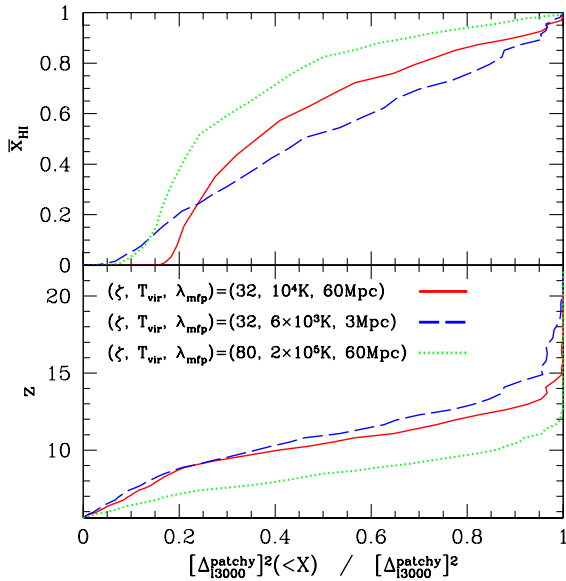


Figure 5. The cumulative fraction of the $z > 5.6$ kSZ signal at $l = 3000$ sourced by redshifts less than z (bottom panel) and corresponding global neutral fractions less than \bar{x}_{HI} (top panel). Three model curves are shown corresponding to: $\{\zeta, T_{\text{vir}}, \lambda_{\text{mfp}}\} = \{32, 10^4 \text{ K}, 60 \text{ Mpc}\}$, $\{32, 6 \times 10^3 \text{ K}, 3 \text{ Mpc}\}$, $\{80, 2 \times 10^5 \text{ K}, 60 \text{ Mpc}\}$.

of the ionizing efficiency, $\zeta = 32[(1+z)/11]^2$. By increasing the efficiency in this model at early times ($z > 10$) and decreasing it at later times ($z < 10$), the ionized structures become more uniform in size, and reionization is extended. The corresponding power spectra at $l = 3000$ (corresponding to $\sim 20 \text{ Mpc}$ structures at high- z) is the largest in this model, $[\Delta_{l3000}^{\text{patchy}}]^2 = 3.3 \mu\text{K}^2$, placing it on the threshold of current measurements. Such a model could be motivated, for example, by an efficient top-heavy IMF in the early universe, transitioning to an inefficient, feedback-regulated star formation regime at later times. We find that models with stronger evolution (e.g., $\zeta = 32[(1+z)/11]^3$) are ruled out by present QSO constraints since reionization fails to complete in time (see our discussion of constraints derived from QSO spectra below). Models in which ζ decreases with redshift result in a more sudden reionization and a smaller kSZ signal.

The model in the third panels of figures 1 and 4 also assumes a constant ζ and T_{vir} as in the top panel. However, this model includes evolution in $R_{\text{mfp}} = 60[7/(1+z)]^3$. This evolution is in rough agreement with extrapolations using the measured trend in the ionizing-photon mean free path from $z \sim 2-4$ (e.g., Prochaska et al. 2009), though extrapolations into the reionization epoch are extremely uncertain. The evolving R_{mfp} model results in similar HII bubble morphology as the non-evolving model in the top panel; however, the end stages are extended.

Finally, the bottom panel corresponds to an extreme scenario, where LLSs strongly suppress the growth of HII regions, resulting in a very extended reionization. The corresponding parameters are $\{\zeta, T_{\text{vir}}, R_{\text{mfp}}\} = \{32, 6.3 \times 10^3 \text{ K}, 3 \text{ Mpc}\}$. Here ionization structures are smaller compared with other models, shifting the peak in kSZ power to smaller scales.

We also point out that there is evidence in all four panels that the power in the higher l -multipoles is sourced from earlier times when the bubbles were smallest (i.e. the blue curves start “peeling off” of the red ones from high- l as the redshift upper limit is decreased). As mentioned above, this is due to the fact that the ionization power peaks on increasingly larger scales as reionization progresses and the HII bubbles grow. Understandably, this trend is least evident in the bottom panel, where HII bubbles are constrained to be small for a longer duration, and the contrast between ionization power on large and small scales is smaller.

As already discussed, our fiducial models do not include redshift evolution of our three astrophysical parameters. However, it is interesting that for most of the models shown in Fig. 4, the majority of the kSZ signal is imprinted over a relatively narrow redshift or, more fundamentally, \bar{x}_{HI} range. We have already noted in §2 that doubling the duration of reionization roughly doubles the signal. More precisely however, the important quantity is not the duration of the entire reionization process, but just of the epoch when ionized structures were of the angular scale of interest. The timing of this epoch is model-dependent, but we see from Fig. 4 that the ionization morphology had notable power on $l \approx 3000$ scales during the early/middle stages of reionization.

To further quantify which epochs source the patchy kSZ signal, in Fig. 5 we plot the fraction of the total $z > 5.6$ kSZ signal at $l = 3000$ sourced by redshifts less than z (bottom panel) and global neutral fractions less than \bar{x}_{HI} (top panel). Three model curves are shown, corresponding to: $\{\zeta, T_{\text{vir}}, R_{\text{mfp}}\} = \{32, 10^4 \text{ K}, 60 \text{ Mpc}\}$, $\{32, 6 \times 10^3 \text{ K}, 3 \text{ Mpc}\}$, $\{80, 2 \times 10^5 \text{ K}, 60 \text{ Mpc}\}$. The extremely extended reionization model shown with the blue dashed curve has kSZ power imprinted smoothly and uniformly throughout reionization, i.e. $d[\Delta_{l3000}^{\text{patchy}}]^2/d\bar{x}_{\text{HI}} \sim 1$. In this case, as is qualitatively evident from the bottom panel of Fig. 1, the ionization structure retains

power on $l = 3000$ ($L \approx 20$ Mpc) scales throughout reionization. However, more standard models are not sensitive to the later stages of reionization, when HII regions grow to be larger than $l = 3000$. The “fiducial” case shown with the solid red curve only has $\approx 20\%$ of the $l = 3000$ reionization signal imprinted in the last half of reionization, $\bar{x}_{\text{HI}} < 0.5$.¹² Models with even larger HII regions, such as the one shown with the dashed green curve, are even less sensitive to the later stages of reionization. In particular, this model has only $\approx 16\%$ of the $l = 3000$ reionization signal imprinted in the last half of reionization. The fact that the kSZ signal is sensitive mostly to the first half of reionization suggests that our astrophysical parameters can be interpreted as the average values during this epoch.

3.2 Signal at $l = 3000$

For the remainder of the paper, we focus our attention of the power at $l \approx 3000$, using the statistic $[\Delta_{l=3000}^{\text{patchy}}]^2 = 3000^2 C_{l=3000}^{\text{patchy}} / (2\pi)$. As discussed in the introduction, these multipoles are the most observable with upcoming and future small-scale CMB observations. At $z \gtrsim 5$, $l = 3000$ roughly corresponds to a physical distance of $\sim \eta 2\pi / l = 20$ Mpc. This suggests that $[\Delta_{l=3000}^{\text{patchy}}]^2$ depends on the timing and duration of ionization structure of comparable scale.

In Fig. 6, we plot $[\Delta_{l=3000}^{\text{patchy}}]^2$ as a function of $\{\zeta, T_{\text{vir}}, R_{\text{mfp}}\}$. Values of $[\Delta_{l=3000}^{\text{patchy}}]^2$ were interpolated from our 103 21CMFAST samples using tessellation-based linear interpolation. Slices through the 3D parameter space are shown at $\zeta = 15, 52$; $T_{\text{vir}} = 10^{3.2}, 10^{5.2}$ K; and $R_{\text{mfp}} = 3$ Mpc (*left panel*). The $[\Delta_{l=3000}^{\text{patchy}}]^2 = 3.5, 2.5, 1.5 \mu\text{K}^2$ contours are plotted in the right panel.

In our parameter space the signal ranges from $[\Delta_{l=3000}^{\text{patchy}}]^2 \approx 1 - 4 \mu\text{K}^2$. The strongest signal in Fig. 6 corresponds to the regime with early, extended reionization scenarios. In other words, high values of $[\Delta_{l=3000}^{\text{patchy}}]^2$ result when reionization is driven by very small galaxies (small T_{vir}) whose contribution is significant (large ζ) so as to start reionization early, and with relatively abundant LLSs (low R_{mfp}), so as to extend the duration of the epochs where HII regions are comparable in size to $l \approx 3000$. These scenarios would be the easiest to observe, and the first to be ruled out with an upper limit on $[\Delta_{l=3000}^{\text{patchy}}]^2$.

There are a couple of interesting non-monotonic trends to note in Fig. 6. The peak in power occurs at $\{\zeta, T_{\text{vir}}, R_{\text{mfp}}\} \sim \{40, 10^3 \text{ K}, 10 \text{ Mpc}\}$. As the ionizing efficiency from this peak is increased, the kSZ power falls somewhat because this change results in reionization occurring more rapidly. Lower efficiencies delay reionization to later epochs, also resulting in a slightly weaker kSZ signal.

Additionally, the smaller the mean free path generally the stronger the signal, since they produce more extended reionization histories. However, the $l = 3000$ power is a maximum for models with $R_{\text{mfp}} \approx 10$ Mpc because this R_{mfp} is roughly the scale probed at this multipole (see left panel Fig. 6), whereas smaller R_{mfp} values suppress structure on this scale.

3.2.1 Including constraints from WMAP and QSOs

Other probes of the reionization epoch can compliment the kSZ signal, and restrict the allowed parameter space. Our two most robust

¹² Note that in this case, $\approx 17\%$ of the $z > 5.6$ signal originates post-reionization, $5.6 < z \lesssim 8.5$, and would be more appropriately classified as the OV component (see the discussion of our conventions at the beginning of §2).

constraints at present come from the Lyman-series forests detected in the spectra of high-redshift QSOs and from the measurement of τ_e by the WMAP satellite.

The Lyman-series forests in high-redshift QSOs, originally detected in the Sloan Digital Sky Survey (SDSS), have been used in recent years to claim that reionization must have been over by $z \sim 6$ (e.g., Fan et al. 2006). Photons emitted by a QSO blueward of the Ly α line can redshift into the Lyman resonances along the LOS and be absorbed by atomic hydrogen (although complete absorption does not necessarily indicate a neutral region since this probe saturates easily; Gunn & Peterson 1965). A model-independent, maximally conservative upper limit on \bar{x}_{HI} can be obtained just from the fraction of pixels in the Lyman- α and Lyman- β forest which are jointly dark (Mesinger 2010b), yielding $\bar{x}_{\text{HI}} \lesssim 0.25$ at $z = 5.6$ (McGreer et al. 2011; McGreer et al., in preparation). Fig. 7 demarcates in gray the surface corresponding to models which have $\bar{x}_{\text{HI}} = 0.25$ at $z = 5.6$. The parameter space on the other side of that surface is robustly ruled out with QSO measurements, and we leave it blank in this and future plots. As expected, QSO constraints rule out models where the sources reside in very rare, massive halos such that reionization is late or those with a significant \bar{x}_{HI} “tail” to lower redshifts owing to a small mean free path.

The other significant constraint on reionization comes from the measurement of the Thompson scattering optical depth to CMB photons. The seven-year WMAP (WMAP7) estimate is $\tau_e = 0.088 \pm 0.015$ (Komatsu et al. 2011). Fig. 7 demarcates the 2σ WMAP7 limits on τ_e with purple surfaces and the 3σ limits with yellow surfaces. We consider the portion of our parameter space not enclosed by the 3σ contours to be robustly ruled out, and we leave it blank in this and future plots. The WMAP7 τ_e limits mainly serve to rule out very early reionization scenarios. These are the models where reionization is driven by very small galaxies. Fig. 7 and Fig. 8 demonstrate that *an upper limit of $[\Delta_{l=3000}^{\text{patchy}}]^2 \lesssim 3.5$ improves on existing 3σ WMAP7 constraints.*

Fig. 8 shows additional slices through the reionization parameter space, to focus on the trends noted above. The top row shows $[\Delta_{l=3000}^{\text{patchy}}]^2$ for cuts at $R_{\text{mfp}} = 60$ and 3 Mpc. Consistent with our previous discussion, $[\Delta_{l=3000}^{\text{patchy}}]^2$ increases with decreasing R_{mfp} (until very low values) as reionization becomes more prolonged.

The middle row of panels in Fig. 8 shows $[\Delta_{l=3000}^{\text{patchy}}]^2$ at $\zeta = 21$ (left panel) and 41 (right panel). Contours of constant kSZ power shift to more massive sources as the ionizing efficiency is increased (i.e. the kSZ signal increases with ζ , since reionization occurs earlier). The non-monotonic trend of $[\Delta_{l=3000}^{\text{patchy}}]^2$ with R_{mfp} is clearly evident in these panels. The signal is not sensitive to the value of the mean free path when $R_{\text{mfp}} \gtrsim 15$ Mpc, since these values are large enough that they do not impact the reionization morphology and the morphology is driven just by the clustering of the sources.

The bottom row of Fig. 8 shows slices at $T_{\text{vir}} = 10^4$ and 10^5 K. A similar structure of the signal is seen as in the top panels, with the signal now decreasing with T_{vir} . High redshift QSOs already rule out most of our parameter space at $T_{\text{vir}} = 10^5$ K. Although slightly fainter than current direct detection limits (from Hubble/WFC3, see e.g., Salvaterra et al. 2011; Finlator et al. 2011), these sources reside in halos massive enough to be rare in the early Universe. If such relatively massive sources drove reionization, it would have to occur at late epochs and occur very rapidly not to violate existing constraints, resulting in a weak patchy kSZ signal, $[\Delta_{l=3000}^{\text{patchy}}]^2 \approx 1 \mu\text{K}^2$. Even so, these scenarios are still ruled out by WMAP7 at $> 2\sigma$.

When viewed at constant τ_e , the reionization signal varies by $d[\Delta_{l=3000}^{\text{patchy}}]^2 \approx 1 \mu\text{K}^2$. If the signal can be determined to such ac-

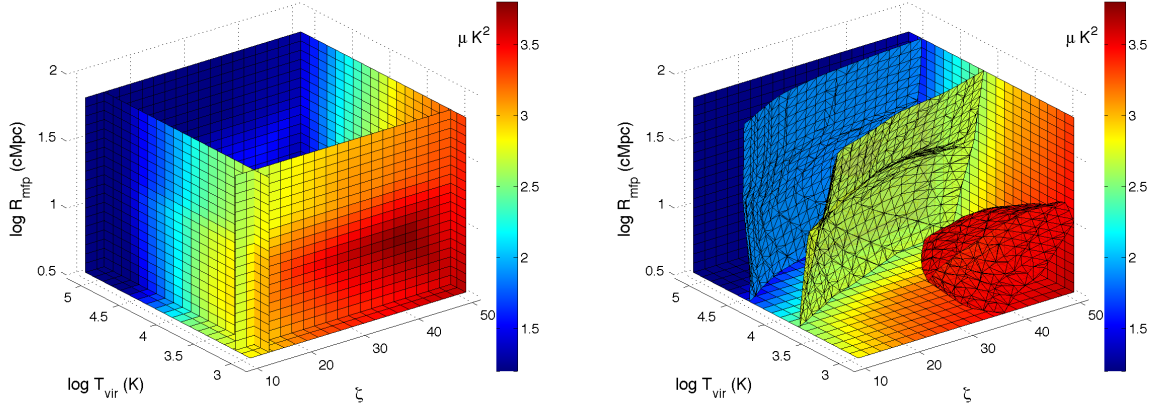


Figure 6. $[\Delta_{l=3000}^{\text{patchy}}]^2$ at $l = 3000$ from inhomogeneous reionization, as a function of our three astrophysical parameters. *Left panel:* Slices through the 3D parameter space are shown at $\zeta = 15$ and 52 ; $T_{\text{vir}} = 10^{3.2}$ and $10^{5.2}$ K; and $R_{\text{mfp}} = 3$ Mpc. *Right panel:* Cuts through the parameter space are shown with $[\Delta_{l=3000}^{\text{patchy}}]^2 = 3.5, 2.5, 1.5 \mu\text{K}^2$.

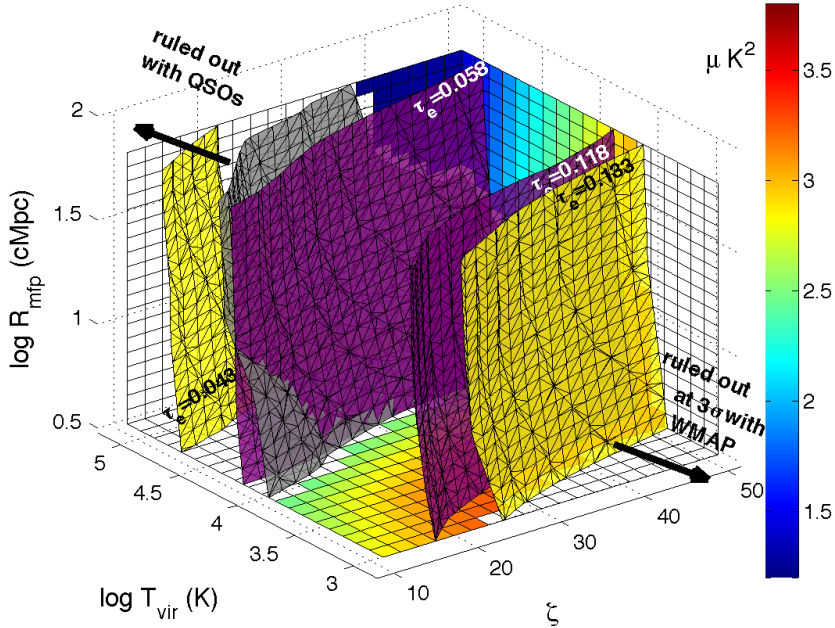


Figure 7. 3D parameter space demarcating regions that are inconsistent with current QSO and WMAP7 τ_e constraints (see text). The gray contour corresponds to models which have $\bar{x}_{\text{HI}} = 0.25$ at $z = 5.6$. The purple (yellow) contours demarcate the 2 (3) σ WMAP7 limits on τ_e .

curacy (see §5), the kSZ would provide *complimentary* information to the mean optical depth statistic. This complementary information can be used to determine the duration of reionization, Δz_{re} , as we shall see below. In our parameter space, the duration of reionization is most sensitive to the mean free path in the range $R_{\text{mfp}} \lesssim 15$ Mpc. Nevertheless, smaller differences of $d[\Delta_{l=3000}^{\text{patchy}}]^2 \sim 0.5 \mu\text{K}^2$ can be obtained by varying just T_{vir} and ζ at fixed τ_e (see the top row of Fig. 8).

3.2.2 Redshift and duration of reionization

Here we cast our patchy kSZ signals in terms of two empirical parameters, which can be easier to interpret than our astrophysical ones:

(i) z_{re} : defined as the redshift at which $\bar{x}_{\text{HI}} = 0.5$,

(ii) Δz_{re} : defined as the redshift interval from $\bar{x}_{\text{HI}} = 0.75$ to $\bar{x}_{\text{HI}} = 0.25$.

Note that by definition Δz_{re} is a change in the HI fraction by $\Delta \bar{x}_{\text{HI}} = 0.5$. The entire process of reionization could be considerably longer owing to extended early and late epochs (e.g., Mesinger 2010a), but the kSZ signal at $l \sim 3000$ is less sensitive to these stages as demonstrated above.

Fig. 9 shows contours of fixed $\Delta z_{\text{re}} = 1.5$ and 3.5 through our astrophysical parameter space. Understandably, rapid reionization scenarios are located in the top, back right corner of this figure: bright sources hosted by massive halos with relatively few LLSs to impede the progress of reionization. The contrary is true for slow

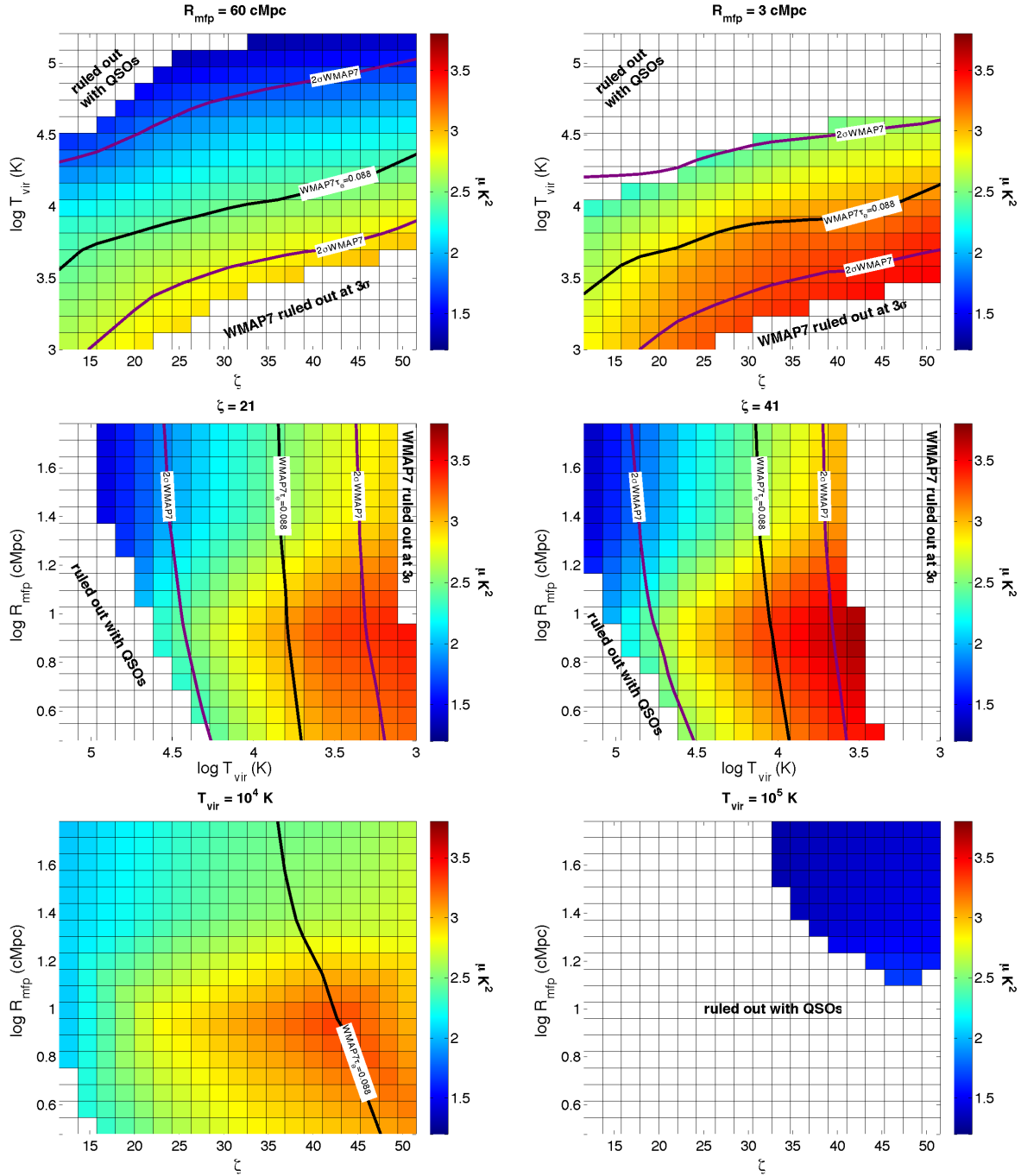


Figure 8. Slices of $[\Delta_{I3000}^{\text{patchy}}]^2$ through our astrophysical parameter space. *Top:* $R_{\text{mfp}} = 60$ and 3 Mpc; *middle:* $\zeta = 21$ and 41 ; *bottom:* $T_{\text{vir}} = 10^4$ and 10^5 K. Also shown are contours at fixed τ_e , corresponding to the preferred WMAP7 τ_e value and its 2σ limits.

reionization models. For clarity of presentation, surfaces of constant z_{re} are not shown; however, they are very similar to the constant τ_e contours shown in the previous figures.

Fig. 10 shows contours of $[\Delta_{I3000}^{\text{patchy}}]^2$ as a function of z_{re} and Δz_{re} . Constant τ_e lines are also depicted. These almost correspond to lines of constant z_{re} , since the reionization histories of our models are relatively symmetric around z_{re} .¹³

¹³ Note that the curving of the lower 2σ limit on τ_e as one approaches high values of Δz_{re} results from the fact that these extreme scenarios (corresponding to late-appearing sources and small mean free paths), have an

asymmetric extended tail to low \bar{x}_{HI} (see Fig. 3). In these models the small mean free path to ionizing photons creates an effective horizon thus delaying the completion of the final (i.e. overlap) stages of reionization, as discussed above (Furlanetto & Mesinger 2009; Alvarez & Abel 2010).

asymmetric extended tail to low \bar{x}_{HI} (see Fig. 3). In these models the small mean free path to ionizing photons creates an effective horizon thus delaying the completion of the final (i.e. overlap) stages of reionization, as discussed above (Furlanetto & Mesinger 2009; Alvarez & Abel 2010).

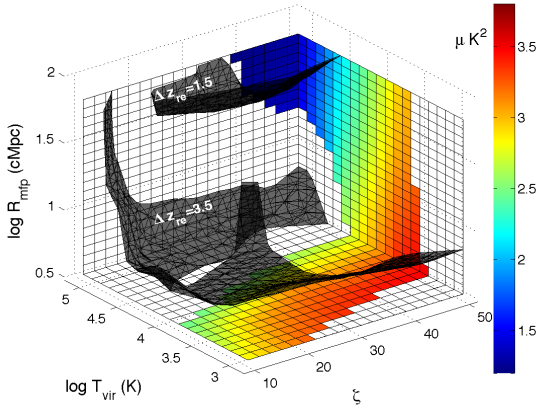


Figure 9. Contours of $\Delta z_{\text{re}} = 1.5$ and 3.5 through our astrophysical parameter space (upper and lower contours, respectively). Note that Δz_{re} is defined as the interval for which $0.25 < \bar{x}_{\text{HI}} < 0.75$, which can be significantly shorter than the duration over a larger range in \bar{x}_{HI} .

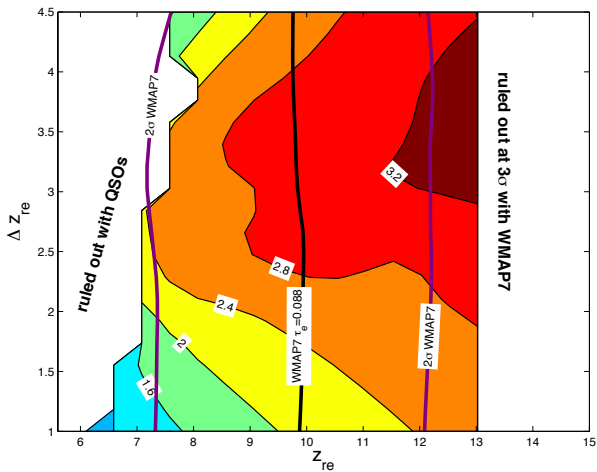


Figure 10. Contours of $[\Delta_{l3000}^{\text{patchy}}]^2$ as a function of z_{re} and Δz_{re} .

$\tau_e = 0.088$ and $[\Delta_{l3000}^{\text{patchy}}]^2 = 2.8\mu\text{K}^2$ allow both $\Delta z_{\text{re}} = 2.3$ and 4.0 . This is primarily due to the fact that the peak of the kSZ power shifts in angular scale.

The *slope* of the patchy kSZ power at $l = 3000$ can break this degeneracy. The slope requires sensitivities that are a few times improved over ongoing measurements that seek to detect the kSZ. This logarithmic slope is plotted in Fig. 11.¹⁴ From this, we see that the longer/earlier reionization scenarios have a positive slope, meaning that the peak in kSZ power occurs on scales smaller than $l = 3000$, which correspond to earlier stages of reionization (see the bottom panel of Fig. 4 and associated discussion). A detection of the sign of this slope, combined with τ_e and $[\Delta_{l3000}^{\text{patchy}}]^2$, should robustly determine z_{re} and Δz_{re} . Furthermore, we find that positive values of the slope come exclusively from models with low values of $R_{\text{mfp}} \lesssim 10$ Mpc. Therefore detecting the sign of the slope can constrain the abundance of absorption systems in the early Uni-

¹⁴ This figure was created with a wider spectral smoothing kernel ($\Delta l = 600$, instead of $\Delta l = 300$ used throughout the rest of the paper). This was done to smooth over small spectral features present in our realization. We find that, unlike $[\Delta_{l3000}^{\text{patchy}}]^2$, the spectral slope as defined above is sensitive to such cosmic variance effects.

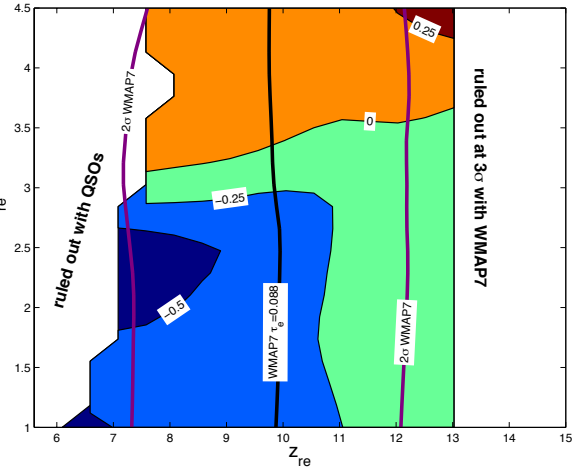


Figure 11. Contours of the logarithmic slope of the power spectrum around $l \sim 3000$. Specifically, the slope is defined as $2 \log[\Delta_{l3000}^{\text{patchy}} / \Delta_{l2700}^{\text{patchy}}] / \log[3300/2700]$.

verse, at redshifts far beyond those of present estimates based on QSO spectra.

4 COMPARISON WITH PRIOR STUDIES

Several studies have investigated the kSZ signal from inhomogeneous reionization using either radiative transfer simulations of reionization or semi-numeric models of this process¹⁵:

- McQuinn et al. (2005) investigated the kSZ from reionization using an analytic framework also based on the Furlanetto et al. (2004) model, by varying the parameter ζ ; Furlanetto et al. (2006) generalized their calculation to include models where the ionizing efficiency depends on halo mass. This analytic method is more approximate than the calculations presented here. However, values of $[\Delta_{l3000}^{\text{patchy}}]^2$ found in McQuinn et al. (2005) are similar to what we find in our analogous models (although, their functional form for $[\Delta_{l3000}^{\text{patchy}}]^2$ is slightly more peaked). However, the mass-dependent ζ -models in Furlanetto et al. (2006) exhibit a stronger l -dependence than we find in our T_{vir} models, which should mimic the same effect. These differences likely owe to the approximations made in their analytic derivations.

- Zahn et al. (2005) calculated the kSZ from two reionization models with a fixed and temporally evolving ζ parametrization using the Zahn et al. (2007) semi-numeric implementation of reionization on top of a 100 Mpc/h SPH simulation. This box size is insufficient to capture the largest-scale velocity modes and, thus, should underestimate the kSZ signal. Furthermore, it is difficult to compare our calculations with theirs owing to their different reionization histories.¹⁶ Nevertheless, we note that their results qualitatively agreed with those of McQuinn et al. (2005) and, by extension, those here.

¹⁵ Most previous studies used a cosmology with $\sigma_8 = 0.9$, which will result in a slightly higher amplitude since the patchy kSZ is proportional to $v^2 \propto \sigma_8^2$. σ_8 primarily affects the timing of reionization, and not the HII morphology (McQuinn et al. 2007).

¹⁶ The Zahn et al. (2007) constant ζ model has a smaller Δz_{re} than ours owing to their implementation.

• Iliev et al. (2007) used full radiative transfer simulations of reionization to calculate the kSZ from a 100 Mpc/h simulation supplemented with a scheme to account for missing large-scale velocity flows. Their power spectra peak at $l \approx 3000$, similar to our constant ζ models, but have 2 – 3 times higher amplitudes. The likely cause of this discrepancy is the presence of a more uniform bubble size in the Iliev et al. (2007) models. This is in contrast with our models and also with other radiative transfer simulations of reionization (e.g., McQuinn et al. 2007; Trac & Cen 2007).

• When our work was nearing completion, a similar study was made public, focusing on reionization timing and duration constraints implied by the two year SPT data (Zahn et al. 2011). They used a reionization model similar to ours, and although detailed comparisons are difficult, their power spectra roughly agree with ours in both shape and amplitude. However, they do not explore the same $(\zeta, T_{\text{vir}}, R_{\text{mfp}})$ parameter space we do. Instead, they only focus on the efficiency parameter, ζ , encoding the sharpness of reionization through an “acceleration” parameter. This effectively allows the ionized fraction to rise much more steeply, $\bar{x}_i \propto (\zeta_0 f_{\text{coll}})^\beta$, where they vary ζ_0 and β in order to sample a wide range of reionization histories. Because of this exponential dependence on the collapse fraction, they are able to generate much sharper reionization histories, useful for their Markov chain Monte Carlo (MCMC) analysis. For example, halving the duration of reionization (and roughly the kSZ power) in a fiducial $T_{\text{vir}} \sim 10^4 \text{K}$, $\zeta_0 \sim 20$ model requires $\beta \sim 2.5$. Although such a parametrization allows for a larger variety of kSZ signals, which can fit the aggressive SPT bounds (see below), we caution that it is not physically motivated. Any reasonable feedback mechanism delays reionization instead of accelerating it (e.g., Thoul & Weinberg 1996; Springel & Hernquist 2003; Pawlik & Schaye 2009).¹⁷ Our work here is complementary to theirs, as we predict the kSZ signal for a wide range of realistic reionization models. We also provide physical insights into the signal, for example showing that the shape of the patchy kSZ signal can be significantly affected by R_{mfp} ; thus $[\Delta_{l3000}^{\text{patchy}}]^2$ and τ_e do not uniquely determine the redshift and duration of reionization. We also demonstrate that the bulk of the patchy signal for most models is sourced by the early-to-middle stages of reionization. Therefore any kSZ-based inferences about the later stages of reionization are indirect and very model dependent.

5 CONTEXT WITH RECENT AND FORTHCOMING OBSERVATIONS

Recently, Reichardt et al. (2011) placed a limit of $[\Delta_{l3000}]^2 < 2.8 \mu\text{K}^2$ at 95% C.L. using two year SPT measurements. This aggressive bound is valid under the assumption that there is no CIB-tSZ correlation. Allowing for such a correlation, the constraint degrades to $[\Delta_{l3000}]^2 \lesssim 6 \mu\text{K}^2$ at 95% C.L.. This is also in agreement with the 1yr data from the ACT, which implies $[\Delta_{l3000}]^2 = 6.8 \pm 2.9 \mu\text{K}^2$ (Dunkley et al. 2011).

Despite the wide parameter space of models we explore, we predict a fairly narrow range for the patchy reionization component

¹⁷ The very first, molecularly cooled galaxies could experience positive/accelerating feedback due to the enhanced free-electron fraction from ionizing photons (e.g., Oh & Haiman 2002) or hydrodynamical shocks (Shapiro & Kang 1987), which catalyzes the formation of molecular hydrogen. Such feedback would be mild, confined to fossil HII regions and edges of ionization fronts (e.g., Ricotti et al. 2002; Kuhlen & Madau 2005), and short-lived (Haiman et al. 2000; Mesinger et al. 2006).

of the kSZ power, $[\Delta_{l3000}^{\text{patchy}}]^2 \approx 1.5\text{--}3.5 \mu\text{K}^2$. When combined with estimates for the homogeneous ionization (OV) component in §2.2 (see also Shaw et al. 2011), $[\Delta_{l3000}^{\text{OV}}]^2 \approx 2\text{--}3 \mu\text{K}^2$, this work implies that the total kSZ power is $[\Delta_{l3000}]^2 \approx 3.5\text{--}6.5 \mu\text{K}^2$. Therefore the recent conservative SPT bound is on the cusp of constraining viable reionization scenarios.

However, the tighter SPT bound, $[\Delta_{l3000}]^2 < 2.8 \mu\text{K}^2$ at 95% C.L., is incompatible with all of our reionization models. Smaller patchy reionization signals than our predicted range, i.e. $[\Delta_{l3000}^{\text{patchy}}]^2 < 1 \mu\text{K}^2$ – as would accommodate this SPT constraint – require very rapid and late reionization histories (i.e., spanning $z \sim 6\text{--}7$). In these, ionizing sources would reside in extremely rare, massive halos ($T_{\text{vir}} \gtrsim 10^6 \text{K}$) such that their abundance grows rapidly with time. However, such models are difficult to accommodate with current constraints: (i) transmission in the Lyman forests of high- z QSOs provides a low- z limit to reionization so that reionization cannot occur too late (e.g., McGreer et al. 2011); (ii) the redshift evolution of the transmission in the Lyman forests favors a slow evolution in the ionizing emissivity and, thus, a more extended reionization process (Miralda-Escudé 2003; Bolton & Haehnelt 2007b); (iii) the luminosity function of high-redshift galaxies (e.g., Bouwens et al. 2008) supports a sizable contribution to reionization by galaxies fainter and more abundant than those observed¹⁸. To illustrate points (i) and (ii) in greater detail, we plot the redshift evolution of the ionizing photon emissivity and \bar{x}_{HI} in Fig. 12. Increasing T_{vir} steepens the redshift evolution of the emissivity. Therefore, even though one can increase the ionizing efficiency to compensate for the paucity of sources (appealing to larger than expected values of $f_* f_{\text{esc}}$ or more exotic, top heavy stellar populations), the evolution of the emissivity becomes too steep to match the data at $3 < z < 6$, in the absence of a rapid counter-evolution of ζ or rapid feedback mechanisms. This is illustrated by the dashed red curve in Fig. 12, corresponding to $T_{\text{vir}} = 10^6 \text{K}$, $\zeta = 300$.

If the more aggressive SPT bound is confirmed, more exotic reionization scenarios that reduce the level of patchiness may become favorable. The most plausible candidates would be very high-energy X-rays with long mean free paths, which would significantly “pre-ionize” the IGM (we show above that the early to mid stages of reionization are the most relevant for the $l = 3000$ signal). A homogeneous ionization floor of amplitude x_i suppresses the kSZ power by the factor $\sim (1 - x_i)^2$ (see Visbal & Loeb 2011 for a simple model of X-ray reionization and the kSZ). For example, if X-rays homogeneously pre-ionize the IGM to $x_i = 0.3$, the patchy signal from our models would decrease to $[\Delta_{l3000}^{\text{patchy}}]^2 \lesssim 0.7\text{--}1.7 \mu\text{K}^2$, with some models accommodating the aggressive SPT bound. The patchy epoch of reionization would also occur quicker given a homogeneous head-start, further decreasing the kSZ signal. However, a homogeneous pre-ionization is also an extreme simplification, as X-rays would still imprint some inhomogeneities on angular scales of $l = 3000$ ($\sim 20 \text{Mpc}$ at high redshifts), given that the majority of X-ray photons have mean free paths much less than the Hubble length even for hard QSO spectra.

In any case, since late-forming massive halos host both hot gas and star forming galaxies, it is likely that the CIB and the tSZ are correlated (e.g., Sehgal et al. 2010). This would invalidate the aggressive $[\Delta_{l3000}]^2 < 2.8 \mu\text{K}^2$ constraint proposed by Reichardt et al. (2011), implying that the more conservative SPT bound of

¹⁸ Note that the observed galaxies roughly correspond to the largest values of $T_{\text{vir}} \sim \text{few} \times 10^5 \text{K}$ used in this study (e.g., Labbe et al. 2010; Salvaterra et al. 2011; Finlator et al. 2011).

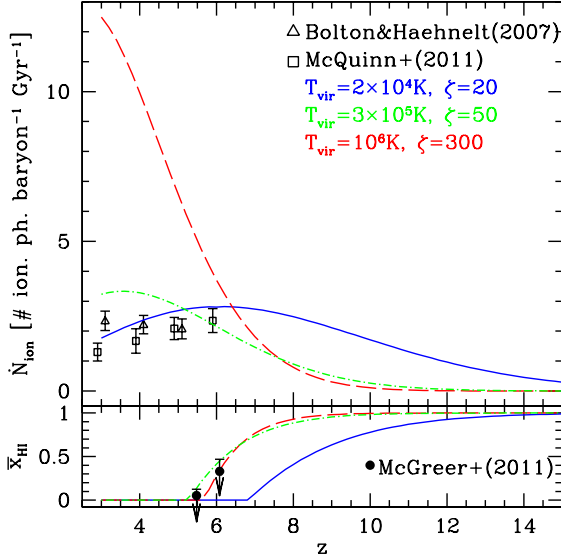


Figure 12. The redshift evolution of the ionizing photon emissivity (*top panel*) and \bar{x}_{HI} (*bottom panel*). Emissivity constraints inferred from the Ly α forest are shown as squares (McQuinn et al. 2011) and triangles (Bolton & Haehnelt 2007b) (offset by $\Delta z = 0.1$ to improve legibility); the maximally conservative neutral fraction constraints from the dark fraction in the Ly α and Ly β forests (McGreer et al. 2011) are shown in the bottom panel. We also show the analytic predictions, $\dot{N}_{\text{ion}} = \zeta(1 + n_{\text{rec}})df_{\text{coll}}/dt$, for three models, assuming $n_{\text{rec}} = 0$ and $R_{\text{mfp}} = \infty$. The solid blue curve corresponds to “standard” parameter choices of $T_{\text{vir}} = 2 \times 10^4 \text{K}$, $\zeta = 20$, and is in agreement with both constraints. As T_{vir} is increased, reionization occurs more rapidly and at later times. To fit the upper limits on \bar{x}_{HI} , this increase in T_{vir} must be accompanied by an increase in ζ . This is illustrated by the green dot-dashed curve, which corresponds to the corner of our parameter space, $T_{\text{vir}} = 3 \times 10^5 \text{K}$, $\zeta = 50$. Increasing T_{vir} also steepens the redshift evolution of the emissivity. Therefore, even though one can increase the ionizing efficiency to compensate for the paucity of sources, the evolution of the emissivity becomes too steep to match the data at $3 < z < 6$, in the absence of powerful and rapid feedback mechanisms or an equally rapid evolution in ζ post reionization. This is illustrated by the dashed red curve, corresponding to $T_{\text{vir}} = 10^6 \text{K}$, $\zeta = 300$.

$[\Delta_{l3000}]^2 < 6 \mu\text{K}^2$ is more plausible. This limit is consistent with all of our reionization scenarios, and is on the cusp of the probing early/extended reionization models. A $\approx 1 \mu\text{K}^2$ constraint on the signal is projected for the coming year (Reichardt et al. 2011), which should result in the first detection of the kSZ.

6 CONCLUSIONS

Observational efforts such as ACT and SPT are beginning to set interesting constraints on the kSZ power spectrum at $l \approx 3000$. This is highlighted by the recent SPT constraint of $[\Delta_{l3000}]^2 < 2.8 \mu\text{K}^2$ (Reichardt et al. 2011; $< 6 \mu\text{K}^2$ when allowing for correlations), as well as the ACT measurement of $[\Delta_{l3000}]^2 = 6.8 \pm 2.9 \mu\text{K}^2$ (Dunkley et al. 2011). A $\approx 1 \mu\text{K}^2$ constraint on the signal is projected for the coming year (Reichardt et al. 2011), which should result in the first detection of the kSZ. Second generation instruments, such as ACTPol and STPPol, will further improve the kSZ measurements in the coming years.

This study calculated the patchy kSZ signal for a suite of ≈ 100 inhomogeneous reionization scenarios, which were gener-

ated using the publicly-available code 21CMFAST. In these models, the contribution of inhomogeneous reionization to the CMB angular power spectrum at $l = 3000$ spans only a factor of four, $[\Delta_{l3000}^{\text{patchy}}]^2 \approx 1\text{--}4 \mu\text{K}^2$, despite the large volume of parameter space covered by the reionization models. The allowed range narrows further to $[\Delta_{l3000}^{\text{patchy}}]^2 \approx 1.5\text{--}3.5 \mu\text{K}^2$ when including current constraints on the reionization history from WMAP and high-redshift quasars. We find that for standard models, the bulk of the signal is imprinted in the early to middle stages of reionization, when the (clustered) ionized structures have angular scales comparable to $l \approx 3000$.

The range $[\Delta_{l3000}^{\text{patchy}}]^2 \approx 1.5\text{--}3.5 \mu\text{K}^2$, combined with estimates for the post reionization kSZ of $[\Delta_{l3000}^{\text{OV}}]^2 \approx 2\text{--}3 \mu\text{K}^2$, results in a total kSZ signal of $[\Delta_{l3000}]^2 = 3.5\text{--}6.5 \mu\text{K}^2$. Thus, the recent conservative SPT bound of $[\Delta_{l3000}]^2 < 6 \mu\text{K}^2$, which assumes a free, scale-independent CIB-tSZ correlation, is on the border of constraining reionization, even assuming conservatively low values for $[\Delta_{l3000}^{\text{OV}}]^2$. The strongest and easiest to detect patchy kSZ signals correspond to early and extended reionization scenarios. In such models, the sources of ionizing photons are abundant at early times and/or there are many recombinations (absorptions in sinks) so that reionization was maximally extended. Furthermore, with the assumption of a slope (but not amplitude) in the CIB-tSZ correlation, Zahn et al. (2011) placed an intermediate upper limit of $[\Delta_{l3000}]^2 \lesssim 4 \mu\text{K}^2$. If such a slope is credible, this constraint is sufficient to rule out our reionization models driven by molecularly-cooled halos (with $T_{\text{vir}} \lesssim 10^4 \text{K}$), and place limits of $z_{\text{re}} \lesssim 10$, $\Delta z_{\text{re}} \lesssim 2$ (see Fig. 10).

On the other hand, the tightest SPT bound $< 2.8 \mu\text{K}^2$ at 95% C.L., which assumes no CIB-tSZ correlation, is incompatible with *all* of our reionization scenarios. Although later and more rapid reionization models might be in agreement with this constraint, it is difficult to push our models to such extremes since these would conflict with other observations of the high-redshift Lyman alpha forest and galaxy luminosity function (LF). This implies that either: (i) the early to middle stages of reionization occurred in a much more homogeneous manner than suggested by the stellar-driven scenarios we explore, such as would be the case if, e.g., very high energy X-rays or exotic particles contributed significantly; and/or (ii) that there is a significant correlation between the CIB and the tSZ, which invalidates these bounds. Upcoming combined analyses of microwave and Herschel far infrared data will likely test the later possibility.

We also find that shape of the patchy kSZ power spectrum encodes astrophysical information. An early and extended reionization in which bubble growth is retarded by recombinations results in a kSZ power spectrum which peaks on smaller scales. The sign of the slope of the patchy kSZ power spectrum at $l \approx 3000$ is useful for discriminating between extended/early and rapid/late reionization processes, which have the same $[\Delta_{l3000}^{\text{patchy}}]^2$. In other words, the values of τ_e and $[\Delta_{l3000}^{\text{patchy}}]^2$ do not uniquely determine the redshift and duration of reionization (c.f., Zahn et al. 2011). However, the sign of the kSZ slope at $l \sim 3000$, combined with τ_e and $[\Delta_{l3000}^{\text{patchy}}]^2$, is sufficient to determine the redshift and duration of reionization. Furthermore, we find that positive values of the slope come exclusively from models with low values of $R_{\text{mfp}} \lesssim 10 \text{Mpc}$. Therefore detecting the sign of the slope can constrain the abundance of absorption systems in the early Universe, at redshifts far beyond those of present estimates based on QSO spectra.

We anticipate that these measurements will be complemented by analyses of the Planck EE signal, which is also sensitive to the

duration of reionization, and potentially by analysis of the contribution of patchy reionization to the CMB polarization power spectrum. Reionization probes not based on the CMB will also yield complementary information, using 21cm tomography, QSO spectra and wide-field LAE studies. These tools will soon reveal the details of the dawn of cosmic structure.

We especially thank Hy Trac for useful discussions, and Andrea Ferrara for comments on an early draft of this paper. We thank Dave Spiegel for his considerable Matlab assistance without which most of the figures presented here would have been much less visually appealing. AM would like to thank the hospitality of Princeton University where most of this work was completed. MM is supported by NASA through an Einstein Fellowship.

REFERENCES

- Abel T., Bryan G. L., Norman M. L., 2002, *Science*, 295, 93
- Ade P. A. R., Aghanim N., Arnaud M., Ashdown M., Aumont J., Baccigalupi C., Balbi A., Banday A. J., Barreiro R. B., Bartlett J. G., et al. 2011, *A&A*, 536, A18
- Alvarez M. A., Abel T., 2010, *ArXiv e-prints*:1003.6132
- Alvarez M. A., Busha M., Abel T., Wechsler R. H., 2009, *ApJ*, 703, L167
- Barkana R., Loeb A., 2004, *ApJ*, 601, 64
- Battaglia N., Bond J. R., Pfrommer C., Sievers J. L., 2011, *ArXiv e-prints*: 1109.3711
- Battaglia N., Bond J. R., Pfrommer C., Sievers J. L., Sijacki D., 2010, *ApJ*, 725, 91
- Bolton J. S., Haehnelt M. G., 2007a, *MNRAS*, 374, 493
- Bolton J. S., Haehnelt M. G., 2007b, *MNRAS*, 382, 325
- Bolton J. S., Haehnelt M. G., Warren S. J., Hewett P. C., Mortlock D. J., Venemans B. P., McMahon R. G., Simpson C., 2011, *MNRAS*, 416, L70
- Bond J. R., Cole S., Efstathiou G., Kaiser N., 1991, *ApJ*, 379, 440
- Bouwens R. J., Illingworth G. D., Franx M., Ford H., 2008, *ApJ*, 686, 230
- Bromm V., Coppi P. S., Larson R. B., 2002, *ApJ*, 564, 23
- Choudhury T. R., Haehnelt M. G., Regan J., 2009, *MNRAS*, 394, 960
- Crociani D., Mesinger A., Moscardini L., Furlanetto S., 2011, *MNRAS*, 411, 289
- Dijkstra M., Mesinger A., Wyithe J. S. B., 2011, *MNRAS*, 414, 2139
- Dijkstra M., Wyithe J. S. B., Haiman Z., 2007, *MNRAS*, 379, 253
- Doré O., Holder G., Alvarez M., Iliev I. T., Mellema G., Pen U.-L., Shapiro P. R., 2007, *PRD*, 76, 043002
- Dunkley J., et al., 2011, *ApJ*, 739, 52
- Dvorkin C., Smith K. M., 2009, *PRD*, 79, 043003
- Fan X., et al., 2006, *AJ*, 132, 117
- Finlator K., Davé R., Özel F., 2011, *ArXiv e-prints*:1106.4321
- Furlanetto S. R., Hernquist L., Zaldarriaga M., 2004, *MNRAS*, 354, 695
- Furlanetto S. R., McQuinn M., Hernquist L., 2006, *MNRAS*, 365, 115
- Furlanetto S. R., Mesinger A., 2009, *MNRAS*, 394, 1667
- Furlanetto S. R., Oh S. P., Briggs F. H., 2006, *Physics Reports*, 433, 181
- Furlanetto S. R., Zaldarriaga M., Hernquist L., 2004, *ApJ*, 613, 1
- Furlanetto S. R., Zaldarriaga M., Hernquist L., 2006, *MNRAS*, 365, 1012
- Gallerani S., Ferrara A., Fan X., Choudhury T. R., 2008, *MNRAS*, 386, 359
- Geil P. M., Wyithe J. S. B., 2008, *MNRAS*, 386, 1683
- Gnedin N. Y., Kravtsov A. V., Chen H.-W., 2008, *ApJ*, 672, 765
- Gruzinov A., Hu W., 1998, *ApJ*, 508, 435
- Gunn J. E., Peterson B. A., 1965, *ApJ*, 142, 1633
- Haiman Z., Abel T., Rees M. J., 2000, *ApJ*, 534, 11
- Haiman Z., Bryan G. L., 2006, *ApJ*, 650, 7
- Haiman Z., Cen R., 2005, *ApJ*, 623, 627
- Haiman Z., Thoul A. A., Loeb A., 1996, *ApJ*, 464, 523
- Hu W., 2000, *ApJ*, 529, 12
- Huffenberger K. M., Seljak U., 2005, *New Astronomy*, 10, 491
- Iliev I. T., Pen U.-L., Bond J. R., Mellema G., Shapiro P. R., 2007, *ApJ*, 660, 933
- Iliev I. T., Shapiro P. R., McDonald P., Mellema G., Pen U.-L., 2008, *MNRAS*, 391, 63
- Kashikawa N., et al., 2006, *ApJ*, 648, 7
- Knox L., Soccimarro R., Dodelson S., 1998, *Physical Review Letters*, 81, 2004
- Komatsu E., et al., 2011, *ApJS*, 192, 18
- Komatsu E., Seljak U., 2002, *MNRAS*, 336, 1256
- Kuhlen M., Madau P., 2005, *MNRAS*, 363, 1069
- Labbe I., et al., 2010, *ApJ*, 708, L26
- Lacey C., Cole S., 1993, *MNRAS*, 262, 627
- Lee K., et al., 2009, *ApJ*, 695, 368
- Ma C., Fry J. N., 2002, *Physical Review Letters*, 88, 211301
- Malhotra S., Rhoads J. E., 2004, *ApJ*, 617, L5
- Malhotra S., Rhoads J. E., 2006, *ApJ*, 647, L95
- Maselli A., Gallerani S., Ferrara A., Choudhury T. R., 2007, *MNRAS*, 376, L34
- McGreer I. D., Mesinger A., Fan X., 2011, *MNRAS*, 415, 3237
- McQuinn M., Furlanetto S. R., Hernquist L., Zahn O., Zaldarriaga M., 2005, *ApJ*, 630, 643
- McQuinn M., Hernquist L., Zaldarriaga M., Dutta S., 2007, *MNRAS*, 381, 75
- McQuinn M., Lidz A., Zahn O., Dutta S., Hernquist L., Zaldarriaga M., 2007, *MNRAS*, 377, 1043
- McQuinn M., Lidz A., Zaldarriaga M., Hernquist L., Dutta S., 2008, *MNRAS*, 388, 1101
- McQuinn M., Oh S. P., Faucher-Giguère C.-A., 2011, *ApJ*, 743, 82
- Mesinger A., 2010a, in M. Raue, T. Kneiske, D. Horns, D. Elsaesser, & P. Hauschildt ed., *Cosmic Radiation Fields How the first generations of luminous baryons established the X-ray and UV backgrounds*. p. 37
- Mesinger A., 2010b, *MNRAS*, 407, 1328
- Mesinger A., Bryan G. L., Haiman Z., 2006, *ApJ*, 648, 835
- Mesinger A., Dijkstra M., 2008, *MNRAS*, 390, 1071
- Mesinger A., Furlanetto S., 2007, *ApJ*, 669, 663
- Mesinger A., Furlanetto S., Cen R., 2011, *MNRAS*, 411, 955
- Mesinger A., Furlanetto S. R., 2008a, *MNRAS*, 385, 1348
- Mesinger A., Furlanetto S. R., 2008b, *MNRAS*, 386, 1990
- Mesinger A., Haiman Z., 2004, *ApJ*, 611, L69
- Mesinger A., Haiman Z., 2007, *ApJ*, 660, 923
- Miralda-Escude J., 1998, *ApJ*, 501, 15
- Miralda-Escudé J., 2003, *ApJ*, 597, 66
- Oh S. P., Haiman Z., 2002, *ApJ*, 569, 558
- Okamoto T., Gao L., Theuns T., 2008, *MNRAS*, 390, 920
- Ostriker J. P., Vishniac E. T., 1986, *ApJ*, 306, L51
- Paardekooper J.-P., Pelupessy F. I., Altay G., Kruij C. J. H., 2011, *A&A*, 530, A87+
- Pawlik A. H., Schaye J., 2009, *MNRAS*, 396, L46
- Peacock J. A., Dodds S. J., 1994, *MNRAS*, 267, 1020
- Péroux C., McMahon R. G., Storré-Lombardi L. J., Irwin M. J., 2003, *MNRAS*, 346, 1103
- Prochaska J. X., Worseck G., O'Meara J. M., 2009, *ApJ*, 705, L113
- Reichardt C. L., et al., 2011, *ArXiv*:1111.0932
- Ricotti M., Gnedin N. Y., Shull J. M., 2001, *ApJ*, 560, 580
- Ricotti M., Gnedin N. Y., Shull J. M., 2002, *ApJ*, 575, 49
- Salvaterra R., Ciardi B., Ferrara A., Baccigalupi C., 2005, *MNRAS*, 360, 1063
- Salvaterra R., Ferrara A., Dayal P., 2011, *MNRAS*, 414, 847
- Santos M. G., Cooray A., Haiman Z., Knox L., Ma C.-P., 2003, *ApJ*, 598, 756
- Santos M. R., Ellis R. S., Kneib J.-P., Richard J., Kuijken K., 2004, *ApJ*, 606, 683
- Sehgal N., Bode P., Das S., Hernandez-Monteagudo C., Huffenberger K., Lin Y.-T., Ostriker J. P., Trac H., 2010, *ApJ*, 709, 920
- Shang C., Haiman Z., Knox L., Oh S. P., 2011, *ArXiv e-prints*
- Shapiro P. R., Kang H., 1987, *ApJ*, 318, 32
- Shaw L. D., Nagai D., Bhattacharya S., Lau E. T., 2010, *ApJ*, 725, 1452

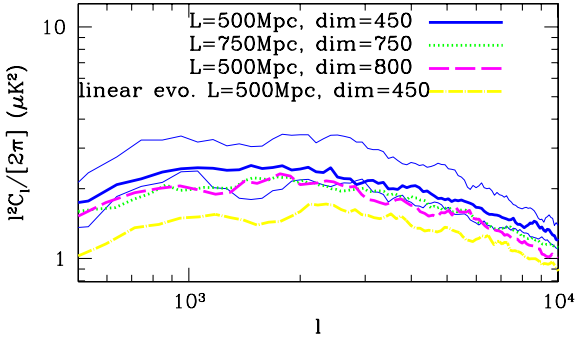


Figure A1. The patchy kSZ power spectra obtained from different simulations. The (thick) solid blue curve corresponds to the same box size and resolution as used in this work: $L = 500$ Mpc on a side, sampled onto a grid with dimensions given by $\text{dim}=450$. The dotted green curve corresponds to a larger box, with comparable resolution: $L = 750$ Mpc, $\text{dim}=750$. The dashed magenta curve has the same box size as our fiducial choice, but with higher resolution, $\text{dim}=800$. The thin solid blue curves show power spectra computed along two basis vectors without rotating the simulation box, for our fiducial choices. Finally, the dot-dashed yellow curve corresponds to the signal computed without PT, just assuming linear evolution of the cosmological fields, such as has been done in previous semi-analytic studies. All curves assume $\{\zeta, T_{\text{vir}}, R_{\text{mfp}}\} = \{32, 10^4 \text{ K}, 30 \text{ Mpc}\}$.

- Shaw L. D., Rudd D. H., Nagai D., 2011, ArXiv:1109.0553
 Songaila A., Cowie L. L., 2010, ApJ, 721, 1448
 Springel V., Hernquist L., 2003, MNRAS, 339, 312
 Stengler-Larrea E. A., et al., 1995, ApJ, 444, 64
 Storrie-Lombardi L. J., McMahon R. G., Irwin M. J., Hazard C., 1994, ApJ, 427, L13
 Su M., Yadav A. P. S., McQuinn M., Yoo J., Zaldarriaga M., 2011, ArXiv e-prints:1106.4313
 Sunyaev R. A., Zeldovich I. B., 1980, MNRAS, 190, 413
 Thoul A. A., Weinberg D. H., 1996, ApJ, 465, 608
 Totani T., Kawai N., Kosugi G., Aoki K., Yamada T., Iye M., Ohta K., Hattori T., 2006, PASJ, 58, 485
 Trac H., Bode P., Ostriker J. P., 2011, ApJ, 727, 94
 Trac H., Cen R., 2007, ApJ, 671, 1
 Valageas P., Balbi A., Silk J., 2001, A&A, 367, 1
 Vale A., Ostriker J. P., 2006, MNRAS, 371, 1173
 Visbal E., Loeb A., 2011, ArXiv e-prints:1109.5722
 Vishniac E. T., 1987, ApJ, 322, 597
 Wise J. H., Cen R., 2009, ApJ, 693, 984
 Wyithe J. S. B., Loeb A., 2004, Nature, 427, 815
 Zahn ., et al., 2011, ArXiv e-prints:1111.6386
 Zahn O., Lidz A., McQuinn M., Dutta S., Hernquist L., Zaldarriaga M., Furlanetto S. R., 2007, ApJ, 654, 12
 Zahn O., Mesinger A., McQuinn M., Trac H., Cen R., Hernquist L. E., 2011, MNRAS, 414, 727
 Zahn O., Zaldarriaga M., Hernquist L., McQuinn M., 2005, ApJ, 630, 657
 Zel'Dovich Y. B., 1970, A&A, 5, 84
 Zeldovich Y. B., Sunyaev R. A., 1969, Astrophys. Space Sci., 4, 301
 Zhang P., Pen U., Trac H., 2004, MNRAS, 347, 1224

APPENDIX A: CONVERGENCE TESTS

Here we briefly quantify the convergence of our numerical results. In Fig. A1, we plot the patchy kSZ power spectra corresponding to the same astrophysical parameter choices, $\{\zeta, T_{\text{vir}}, R_{\text{mfp}}\} = \{32, 10^4 \text{ K}, 30 \text{ Mpc}\}$, but with different simulation box sizes, L , and grid dimensions, dim . The (thick) solid blue curve corresponds to the same box size and resolution used in this work. The dotted green curve corresponds to a larger box, with comparable

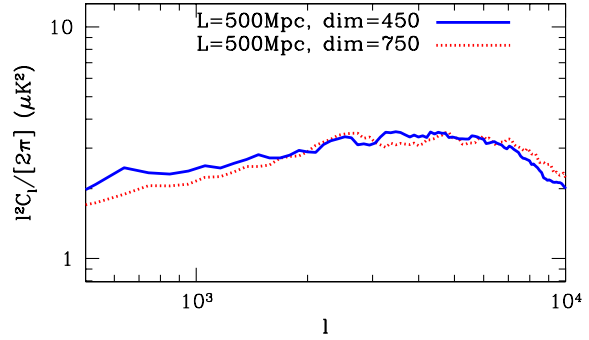


Figure A2. The kSZ signal corresponding to $\{\zeta, T_{\text{vir}}, R_{\text{mfp}}\} = \{32, 6.3 \times 10^3 \text{ K}, 3 \text{ Mpc}\}$ from our fiducial simulation (solid blue curve) and a higher resolution, $\text{dim}=750$ simulation (dotted red curve).

resolution, while the dashed magenta curve has the same box size as our fiducial choice, but with higher resolution. Comparing the blue curve to the magenta and green ones, suggests that our fiducial choices result in a slight overestimate of kSZ power spectrum for this random seed, but have converged to within 10% over the relevant multipoles.

The thin solid blue curves in Fig. A1 show power spectra computed along two basis vectors without rotating the simulation box. From their disparity, one can see that the variance of the velocity fields on scales larger than our $L = 500$ Mpc scales is 10% (Fig 7, Iliev et al. 2007), requiring box rotations to avoid coherently stacking the signal. Finally, the dot-dashed yellow curve corresponds to the signal computed without PT, just assuming linear evolution of the cosmological fields, such as has been done in previous semi-analytic studies (McQuinn et al. 2005). Ignoring non-linearity results in a $\sim 30\%$ underestimate of the $l \sim 2000$ – $10,000$ kSZ power in this model.

One might also worry that our fiducial resolution, with a cell size of 1.1 Mpc, is insufficient to accurately capture the kSZ signal from our low- R_{mfp} models. To test whether this resolution limit has a quantitative impact on our results, we ran a higher resolution, $\text{dim}=750$, run with the same astrophysical parameters as the model shown in the bottom panel of Fig. 1: $\{\zeta, T_{\text{vir}}, R_{\text{mfp}}\} = \{32, 6.3 \times 10^3 \text{ K}, 3 \text{ Mpc}\}$. We compare their kSZ power spectra in Fig. A2, and find that the signal has converged.